Characterisation of premature cell senescence in Alzheimer's disease using single nuclear transcriptomics

Nurun N Fancy[1,4#], Amy M. Smith[1,2,4#], Alessia Caramello[1,4], Stergios Tsartsalis[1,3], Karen Davey[1,4,5], Robert C. J. Muirhead[1,4,5], Aisling McGarry[1,4,7], Marion H. Jenkyns[1], Eleonore Schneegans[1,4], Vicky Chau[1,4], Michael Thomas[1,4], Sam Boulger[1,4], To Ka Dorcas Cheung[1,4], Emily Adair[1,4], Marianna Papageorgopoulou[1,4], Nanet Willumsen[1,4], Combiz Khozoie[1,4], Diego Gomez-Nicola[6], Johanna S Jackson[1,4], and Paul M. Matthews[1,4]*

Department of Brain Sciences, Imperial College London, United Kingdom[1]; Centre for Brain Research and Department of Pharmacology and Clinical Pharmacology, University of Auckland, Auckland, New Zealand[2]; Department of Psychiatry, University of Geneva, Switzerland[3]; UK Dementia Research Institute Centre, Imperial College London, United Kingdom[4]; UK Dementia Research Institute Centre, Kings College London, United Kingdom[5]; School of Biological Sciences, University of Southampton[6]; Department of Basic and Clinical Neuroscience, Institute of Psychiatry, Psychology and Neuroscience, King's College London, London, UK[7]

#Authors contributed equally

Address for correspondence:
Prof. Paul M. Matthews
E515, Department of Brain Sciences
Imperial College London
Hammersmith Hospital
DuCane Road, London WC12 0NN
Tel: 0044 207 594 2612

p.matthews@imperial.ac.uk

Abstract: 139 words
Main text: 5114 words
Tables: 2
Figures: 7
Supplementary Tables: 13
Supplementary figures: 14

Abstract

Aging is associated with cell senescence and is the major risk factor for AD. We characterized premature cell senescence in *post mortem* brains from non-diseased controls (NDC) and donors with Alzheimer's disease (AD) using imaging mass cytometry (IMC) and single nuclear RNA (snRNA) sequencing (>200,000 nuclei). We found increases in numbers of glia immunostaining for galactosidase beta (>4-fold) and $p16^{INK4A}$ (up to 2-fold) with AD relative to NDC. Increased glial expression of genes related to senescence was associated with greater β-amyloid load. Prematurely senescent microglia downregulated phagocytic pathways suggesting reduced capacity for β-amyloid clearance. Gene set enrichment and pseudo-time trajectories described extensive DNA double-strand breaks (DSBs), mitochondrial dysfunction and ER stress associated with increased β-amyloid leading to premature senescence in microglia. We replicated these observations with independent AD snRNA-seq datasets. Our results describe a burden of senescent glia with AD that is sufficiently high to contribute to disease progression. These findings support the hypothesis that microglia are a primary target for senolytic treatments in AD.

Keywords

Aging, senescence, glia, Alzheimer's disease, microglia, oligodendroglia, astrocyte, neuron, single cell transcriptomics, image mass cytometry, cell stress, senolytics.

Introduction

Alzheimer's disease (AD) is the most prevalent form of late-life dementia. It is characterized neuropathologically by extracellular deposits of β-amyloid and intracellular neurofibrillary tangles accompanied by microgliosis, astrogliosis, markers of pan-cellular mitochondrial and lysosomal dysfunction and neurodegeneration [63, 74, 76]. Ageing is the greatest risk factor for AD [26, 53, 60] and is associated with cellular senescence. Accumulation of senescent cells in aging tissues can be accelerated by a wide range of cell stressors, including chronic inflammation [27].

Cell senescence characterized by an irreversible state of cell cycle arrest after proliferative cells reach the so-called "Hayflick limit" is known as replicative senescence [28]. However, premature senescence also is observed with chronic stressors in both proliferative and post-mitotic cells in association with chronic oxidative stress or mitochondrial dysfunction and the induction of DNA damage [5, 25, 35, 59]. Expression of a senescence-associated secretory phenotype (SASP) with senescence in either context can initiate inflammatory responses and propagate locally with release of paracrine mediators [14]. Increased lysosomal β-galactosidase (*GLB1*) and the DNA damage repair protein $p16^{INK4A}$ (p16, encoded by *CDKN2A*) are commonly used immunohistological biomarkers of senescence [41].

Recent evidence has shown that pathological stressors can induce cell senescence in AD to levels above that seen with healthy aging. More than one mechanism may contribute to this. $A\beta_{1–42}$ can induce senescence in astrocytes *in vitro and* greater numbers of p16-positive astrocytes have been reported in the frontal cortex of AD patients compared to that from non-diseased control brains [3]. Increased numbers of p16-positive astrocytes and microglia also have been reported with tau-mediated disease initiation and progression in a mouse model [8]. Associations of premature senescence with both oligodendrocyte progenitor cells (OPCs) [80] and microglia [32] in the APP/PS1 mouse and in *post mortem* AD samples have been described, along with evidence linking microglial senescence to increased replicative stress with aging and β-amyloid triggered generation of disease-associated microglia (DAM) [32, 49]. However, features of premature senescence associated particularly with DNA double-

strand breaks (DSBs) and p16 expression also have been described in post-mitotic cells such as neurons[16, 18, 29].

Despite previous evidence of premature senescence of glia with AD, their aggregate burden, the cells most affected and the mechanistic triggers for senescence in them have not been well described. Here we have comprehensively characterized senescence in *post-mortem* human brain tissue from entorhinal, middle temporal and somatosensory cortices of non-diseased control (NDC) and AD donor brains. We used convergent methods based on immunostaining and distinct transcriptomic analyses, as well as confirmatory analyses of publicly available transcriptomics datasets, to enhance confidence in our findings. We found evidence for increased senescence in AD brains compared to NDC in microglia and more partial senescence signatures in oligodendrocytes, and astrocytes, but little evidence for this in OPCs or neurons. We showed a direct association between β-amyloid accumulation and microglial senescence and provide evidence for its potential functional significance with evidence that senescence reduces transcriptomic signatures of phagocytosis for β-amyloid clearance. Finally, we distinguished mechanisms potentially responsible for initiating senescence pathways in the microglia as a foundation for the design of future senolytic therapies.

Results

Increased expression of markers of cellular senescence in glia in AD

We performed imaging mass cytometry (IMC) on *post mortem* cortical tissue from the middle temporal gyrus (MTG) of neuropathologically diagnosed AD and non-diseased control (NDC) donors of similar ages (Cohort-1: n = 10 from each group, NDC: Braak stage 0–II, AD: Braak stage V–VI, Supplementary data S1) to assess the co-localization of cell-type specific protein markers (microglia, IBA1; oligodendrocyte lineage, OLIG2 [72]; astrocyte, GFAP; endothelial cell, GLUT1; neuron, MAP2) with GLB1, which encodes β-galactosidase, a marker for senescence-associated increases in lysosomal content [42], and with p16, a marker of DNA damage [51]. We found 4.1-, 4.6- and 4-fold more $GLB1^{+}$ microglia (p-value = 0.033), oligodendrocytes (p-value = 0.0031) and astrocytes (p-value = 0.02), respectively, in cortical tissue from donors with AD compared to NDC (Fig. 1a-b, Supplementary fig. 1a-c, Supplementary data S1). We found a 1.6-fold increase in p16 positive microglia with AD compared to

NDC (p-value = 0.01) (Fig. 1b, Supplementary fig. 1a-c) but no significant differences between numbers of p16 positive oligodendrocytes (1.1-fold, p-value = 0.32) or astrocytes (1.3-fold, p-value = 0.31) were found. No differences were found in the numbers of $GLB1^+$ endothelial cells and MAP^+ neurons between AD and NDC (Supplementary fig. 1d).

To understand the correlations between disease stages and activation of senescent pathways across cell types, we extended our findings by performing IMC with a larger panel of antibodies on a second cohort consisting of AD and non-diseased control (NDC) donors from a broader range of Braak stage (Cohort-2, NDC: Braak stage 0–II, AD: Braak stage III–VI, Supplementary data S2). We obtained data from entorhinal cortex (EC, which had the highest pTau/β-amyloid pathology load of the tissues studied from each brain), middle temporal gyrus (MTG, which had a moderate pTau/β-amyloid pathology load) and somatosensory cortex (SSC, which showed the lowest relative pTau/β-amyloid pathology load) from NDC (n = 8) and from donors with neuropathologically defined AD (n = 9). We included an antibody for $p21^{CIP1}$ (p21, encoded by *CDKN1A*), that functions to maintain the viability of DNA damage-induced senescent cells and one for γ-H2AX, a marker of DNA double-strand breaks (DSBs) [2, 79]. Because of the larger number of samples and antibodies in the panel, we used the automated image analysis method SIMPLI for processing this set of IMC images [7]. Using single-cell segmentation, we classified 19,947 cells which were grouped into 15 distinct cell clusters following unsupervised clustering (Fig. 1c). Based on the marker expression profiles, we assigned clusters to major cell types, excluding those expressing more than one cell type marker (Iba1+ microglia, cluster-1, 9; GFAP+ astrocytes, cluster-7; OLIG2+ oligodendrocyte lineage, cluster-2, 3, 6; MAP2+ neuron, cluster-4, 5, 8; GLUT1+ endothelial cells, cluster-0, 11, 13) (Fig. 1d).

We compared the proportion of cells expressing senescence markers (p16, p21, GLB1 and γ-H2AX) in each cluster and found that cluster-9 representing microglia ($Iba1^+$) was both enriched for β-amyloid (Fig. 1d) and had an increased proportion of senescent nuclei expressing GLB1, p21 and γ-H2AX in AD compared to NDC in MTG following a similar trend as we observed in Cohort-1 (p-value < 0.1, Fig. 1e, supplementary fig. 2a). We found increased numbers of $OLIG2^+GLB1^+$ (cluster-3) in the MTG, similar to our findings in Cohort-1 (p-value < 0.1, Fig. 1b, e). We also found

increased numbers of cells expressing γ-H2AX and p21 in one neuronal cluster in the EC (cluster-5) (p-value < 0.1, Supplementary fig. 2b) providing evidence for responses to DSB in neurons independent of other senescence marker proteins. We did not find any cluster to be enriched specifically in AD compared to NDC (Supplementary fig. 3a, b) suggesting the increased proportion of senescent microglia was not due to increased cell population. This confirmed a comprehensive profile of expression of senescence markers in microglia and suggested an association with β-amyloid in AD. Only a single senescence marker was expressed in oligodendroglia and markers of DSB (associated with oxidative DNA damage) were found only in a sub-population of neurons.

Senescence-associated gene expression increases in microglia with AD

We then performed single-nuclei RNA sequencing (snRNAseq) of cortical tissue from *post-mortem* brains (Cohort-2, as used for the IMC shown in Fig. 1c-e, NDC: Braak stage 0–II, AD: Braak stage III–VI, Supplementary data S2) to extend our characterization of cell senescence phenotypes with AD.

After rigorous quality control of the snRNAseq dataset (see Methods), 203,970 nuclei from seven major brain cell types were available for study (Fig. 2a-b, Supplementary fig. 4a, Supplementary data S2). We assessed the relative enrichments of the "canonical senescence pathway (CSP)", "senescence initiating pathway (SIP)" [16] and of senescence associated secretory phenotype (SASP) transcripts for each of the cell-type specific clusters generated from the total set of AD and NDC brain nuclei. We found that the average expression of individual senescence gene was most in microglia (e.g., *ATM*, *RB1*, *NFATC2* and *GLB1*) (Fig. 2c). Astrocytes showed low levels of TP53 (encoding p53) and GLB1 transcript expression. Oligodendrocytes, OPCs and vascular cells showed the lowest expression of senescence pathway gene transcripts, with the exception of *CDKN1A* (encoding p21) which was highly expressed in vascular cells. Only very low levels of *GLB1* transcripts were expressed in neurons. These observations of individual genes were consistent with a relative enrichment for expression of the CSP in these cells: only microglia showed a significant (Wilcoxon test, p-value = 0.0087) increase of CSP gene set expression in AD relative to NDC (Fig. 2d, e). We then calculated the proportions of nuclei expressing CSP (senescent nuclei) as described in [16] and found an increase in the proportion of senescent nuclei

with AD only for microglia in the MTG an observation consistent with our imaging mass cytometry observations (Fig. 2f, Supplementary fig. 4b). Additionally, increased proportion of senescent nuclei was also observed in SSC (Fig. 2f).

We tested for increased, cell-specific expression of genes and pathways associated with chronic stress that could trigger the initiation of senescence in AD [59]. Differential expression analysis confirmed upregulation of DNA damage response genes (*DDB2, RRM2B*) and cellular senescence genes in microglia (*CDK6, MDM2, SMAD2*) with AD relative to NDC (Fig. 3a, b Supplementary data S3). Gene Ontology (GO) enrichment analysis defined upregulation of genes in microglia associated with the p53 signaling pathway, regulation of actin cytoskeleton reorganization and the positive regulation of phosphatidylinositol 3-kinase signaling in addition to those for the cellular senescence pathway (Fig. 3b, Supplementary data S4). Downregulated genes in microglia were enriched for phagocytosis-related pathways (Fig. 3c), consistent with previous reports describing reduced phagocytic capacity of senescent microglia with ageing [57]. Pathways involved in trophic (e.g., “axonal transport”, “synaptic plasticity”) and metabolic support (e.g., “cholesterol and lipid homeostasis”) for neurons were downregulated in astrocytes, oligodendrocytes and OPCs. We did not find enrichment of any senescence related pathways in neurons. Instead, transforming growth factor beta (TGFβ)-related and the neuronal apoptosis pathway genes were upregulated with AD (Supplementary fig. 5a-f, Supplementary data S3, S4).

We then tested for relative senescence gene set enrichment across these cell types using previously defined senescence and related pathways (see Methods for a description of gene set selections) (Supplementary data S5). The “canonical senescence pathway (CSP)” was significantly upregulated in microglia and oligodendroglia and the “regulation of cellular senescence” pathway was significantly upregulated in oligodendroglia in AD compared to NDC. Pathways for “regulation of mitochondrial depolarization” and “regulation of mitochondrial membrane permeability” also were upregulated in microglia (Fig. 3d).

Premature senescence in microglia with AD is associated with increased β-amyloid

We hypothesized that the activation of senescence pathways in AD could be triggered by chronic oxidative stress from interactions with β-amyloid species [9]. Using our IMC images from cohort-1, we tested this hypothesis first by exploring whether microglia near β-amyloid plaques (peri-plaque, where highest exposures to β-amyloid may occur) more frequently express markers of increased senescence relative to microglia far from plaques (non-plaque). A co-localization analysis revealed more than 25% of microglia within 10 µm of β-amyloid plaques in AD showed expression of GLB1 while only 3% of microglia >10 µm distant from plaques expressed this or other senescence markers (Fig. 4a, b, Supplementary data S1).

To validate an association between increased senescence and β-amyloid using the snRNAseq data, we performed a regression analysis for individual gene expression related to increasing loads (log_2FC/% area) of immunostained ($4G8^+$) β-amyloid in paired tissue sections from the contralateral (cryopreserved) hemispheres of each brain (Extended Method Figure 1, Supplementary data S2) for each of the cell types. Transcripts for senescence associated genes including *YPEL3,* which encodes a protein downstream of p53 in the senescence pathway induced by DNA damage [36], *IQGAP2, IL15, AXL, PIK3R1, CDK6, PECAM1 and CXCL16* were significantly upregulated in microglia with increasing β-amyloid load (Fig. 4c, d) [61]. *GLB1* and *MRAS*, a senescence regulator, were upregulated in astrocytes. Oligodendrocytes also upregulated senescence associated genes (*CDK6, CDKN1C, ITPR1*), but we could not detect upregulation of genes associated with senescence in OPCs, neurons or in vascular cells with increased tissue β-amyloid (Fig. 4c, Supplementary data S6). We then tested for β-amyloid or Braak stage associated increases in senescence pathways in glia using gene set enrichment analyses. Microglia showed a significant upregulation of senescence, mitochondrial and endoplasmic reticulum (ER) stress related gene sets for the “canonical senescence pathway (CSP)”, “senescence initiating pathway”, “regulation of cellular senescence” and “regulation of endoplasmic reticulum stress-induced intrinsic apoptotic signaling pathway” with greater β-amyloid and increasing Braak stage (Supplementary fig. 6a-c, Supplementary data S5). Interestingly, “regulation of mitochondrial membrane depolarization”, which included

LRRK2 and *BCL2* genes, both of which can regulate apoptotic cell death pathways, was upregulated with increased β-amyloid [64]. Oligodendrocytes upregulated pathways for "senescence initiators", "regulation of cellular senescence" and "intrinsic apoptotic signaling pathway in response to endoplasmic reticulum stress" and astrocytes upregulated the "senescence initiating pathway" (Supplementary fig. 6a). Upregulation of CSP was found in oligodendrocytes when contrasted between AD and NDC (Fig. 3d) but not associated with β-amyloid suggesting the expression of full senescence phenotype in oligodendrocyte may not be pathology driven.

We did not find evidence for an increase in senescence gene set expression in OPC. We found little evidence for drivers of senescence of neurons, although we found a significant albeit to low level upregulation of "senescence initiating pathway" genes in inhibitory neurons (Supplementary fig. 6a) with increased β-amyloid (Supplementary data S5). Together, these data thus describe comprehensive activation of a senescence transcriptional programme in microglia, expression only for senescence initiation pathways in astrocytes and oligodendroglia, and little evidence even for this amongst OPC and neurons.

We validated these observations using independent snRNAseq data for microglia and astrocytes enriched by FACS sorting. Differentially expressed transcripts in each cell type were identified by regression analysis against $4G8^{+}$ β-amyloid levels. We found increased numbers of senescence genes upregulated in both microglia (*YPEL3*, *IQGAP2, SQSTM1*) and astrocytes (*GLB1, SQSTM1, MRAS*) with greater levels of tissue β-amyloid densities [66] (Supplementary fig. 7a, b, Supplementary data S7). Finally, we conducted a meta-analysis using published single-nucleus RNA sequencing (snRNA-seq) datasets using the "canonical senescence pathway (CSP)" [16] gene set in microglia. Our analysis, which was based on 14 datasets, confirmed significant upregulation of this pathway in microglia for the vast majority of these (12/14, p-value = 7e-04, Supplementary fig. 7c, Supplementary data S8).

Senescence is a cell response to aging. We therefore formally tested for interactions between age and the β-amyloid pathology-associated senescence with AD in the datasets we used for the meta-analyses described above. First, we examined the NDC

samples from our meta-analysis (who had an age range between 50-100 years old). Our findings revealed an increase in the expression of the CSP gene set with healthy aging in microglia; we found an apparent increase from 50-84 years of age in microglia (Supplementary fig. 7d), to reach an apparent plateau. This finding is in agreement with an earlier report in which the authors calculated microglial cell-cycle length and concluded that human microglia reach the Hayflick limit for replicative senescence by the age of ~80 years [1]. However, when we compared microglia from donors with AD to those from NDC, the age association was no longer observed (linear-plateau modelling, Control; p-value = 1.2e-05, AD; p-value = 0.1). We interpret this as evidence that the dominant determinants of senescence in microglia with AD are disease-associated cell stressors (e.g., β-amyloid pathology) rather than chronological aging (Supplementary fig. 7d).

Identification of cell-specific triggers to initiation of senescence

We then explored biological pathways whose expression was enriched with increased β-amyloid load and these glial signatures of premature senescence or its initiation [10, 15]. We found lipid transport and homeostasis related inflammatory responses, cell migration, NF-kappa B signaling, p53 signalling pathway, regulation of cellular senescence, “negative regulation of oxidative stress-induced cell death” pathway upregulation and downregulation of G1/S transition of mitotic cell cycle in microglia, suggesting increased lipid metabolism, inflammatory response and cell cycle arrest were associated with premature senescence in response to greater β-amyloid load. Both oligodendrocytes and astrocytes upregulated genes enriched for lipid metabolism and NF-kappaB signaling pathways. However, the pathways expressed varied between cells, e.g., upregulated genes in oligodendrocytes were associated with interleukin-1-mediated signaling pathway, while those in astrocytes were associated with more general reactive and migratory astrocytic responses (e.g., *ACTN4, EGFR, SASH1*) [43, 78]. (Supplementary fig. 8a, b, Supplementary data S9). In summary, microglia exhibited upregulation of pathways related to β-amyloid response, cell proliferation and migration, and senescence while oligodendrocytes upregulated lipid metabolism and NF-kappaB signaling pathways related to cellular inflammation and astrocytes showed evidence only for general activation and migration.

Sub-populations of microglia and oligodendroglia are differentially susceptible to premature senescence with AD

Glia dynamically adopts different cell states that can be transcriptomically and functionally distinguished. We hypothesized that sub-populations of glial are differentially susceptible to premature senescence with AD. To test this, we subclustered microglia, oligodendrocytes and astrocytes into transcriptomic sub-populations distinguished by previously described marker genes [23, 33, 58].

We identified six microglial sub-populations. Micro1, Micro2, Micro4, Micro5 sub-populations corresponded to previously identified HM_0, GPNMB_EYA2/LPL_CD83, CRM_CCL3 and HM_4 microglial phenotypes, respectively (Fig. 5a, Supplementary fig. 9a-c) [23]. Micro3 showed similarities to HM_3, HM_4 phenotype but also expressed *APOE*, apoptosis associated genes *XAF1, YWHAB, YWHAG, YWHAE* encoding 14-3-3 protein subunits, cell-cycle and cell division control genes *CDK12, MIS18BP1, TAF1D, BOD1L1* and *CCAR1* [6, 30, 67]. This microglial nuclei sub-population expressed fewer total genes and an increased percentage of mitochondrial genes relative to other sub-populations (Supplementary fig. 9a, d, e) [54]. We also identified microglia population (cycMicro) that appeared to be actively proliferating as defined by the expression of multiple centromere proteins (*CENPF, CENPK, CENPU*), mitotic checkpoint kinase (*BUB1B*) and regulator (*CLSPN*), similar to the proportion estimated previously to be in S phase by Ki67 immunohistology [1] (Fig. 5a, Supplementary fig. 9a; Supplementary data S10). The relative numbers of Micro2 nuclei were increased both with AD and with increased amyloid levels (Fig. 5b; logistic mixed-effect model, ** p-value <= 0.01, absolute log2(odds ratio-OR) > 2, Fig. 5c, Wilcoxon rank-sum, p-value = 0.004, Fig. 5d; Pearson's correlation R = 0.63, p-value = 1.4e-06).

The senescence gene set was more highly expressed in Micro1 and Micro2 nuclei from AD brains relative to controls (Fig. 5e). This was not found for other sub-populations. We then calculated the fractions of individual nuclei in each sub-population that were enriched for CSP gene set expression [16]. The fraction of Micro1 nuclei enriched for CSP gene sets in AD was greater than in control tissue (Fig. 5f, Wilcoxon rank-sum, p-value < 0.01) and this fraction increased in Micro1 nuclei in

proportion to the tissue β-amyloid loads (Fig. 5g, Pearson's correlation R= 0.34, p-value = 0.021). Higher proportions of nuclei from the MTG expressed senescent gene sets than from the EC or SSC (Supplementary fig. 9 f, g). Together, these analyses thus provide evidence for increased senescence with AD and increasing β-amyloid specifically amongst that HM (Micro1) and GPNMB_EYA2/LPL_CD83 (Micro2) sub-populations.

Finally, to test whether senescence in AD depends specifically on microglial activation with β-amyloid, we generated snRNA transcriptomes of microglia obtained from neuro-pathologically defined AD donors carrying the *TREM2 R47H* variant allele, which is associated with reduced responsiveness of microglia to β-amyloid [68, 83]. We found a reduced senescence gene signature in microglia from donors carrying the *TREM2 R47H* variant allele relative to the *TREM2* common allele, consistent with our hypothesis of β-amyloid driven senescence activation (Fig. 5h). We did not detect differences in the senescence gene set expression in nuclei from these donors when stratified by either *APOE* or *CD33* genotype (Supplementary fig. 9h, i). As TREM2 acts as a β-amyloid receptor, this suggests that drivers of senescence in microglia are downstream of β-amyloid induced microglial activation.

We used the same approaches to explore senescence in oligodendrocyte and astrocyte sub-populations (Fig. 6, Supplementary fig. 10, Supplementary data S10). There were seven distinguishable sub-populations of oligodendroglia in addition to the committed oligodendroglia precursors (COP). We compared the transcriptomics profile of our oligodendrocyte sub-populations with those from the previous studies[33, 48]. Oligo1 and Oligo2 showed similarities with COPs and OPCs suggesting these subpopulations are not fully matured oligodendrocytes (Fig. 6a, Supplementary fig. 10a, b). While Oligo3 represents a mature myelin forming oligodendrocytes, Oligo4 and Oligo7 resemblance to a mature but non-myelin forming oligodendrocytes. Finally, Oligo5 shows similarities to the end state of oligodendrocyte maturation as identified in[33]. Interestingly, Oligo1 and Oligo4 which showed signatures of imOLGs have increased senescence gene set expression with AD (Fig. 6b). As we found for microglia, specific sub-populations of immature oligodendroglia had evidence for

increased senescence geneset expression, although we could not find a specific association with β-amyloid load.

Finally, we also explored senescence pathway expression in the six astroglial sub-populations that we described previously [66], but did not find that any of these sub-populations showed greater expression of the senescence gene set with AD (Fig. 6c, d, Supplementary fig. 10c).

Mechanisms of microglial activation by β-amyloid promote premature senescence

Senescence and apoptosis both can be triggered by aging and chronic cell stress[13, 24]. To more specifically explore whether senescence with AD includes a contribution from pathology independent of age, we directly correlated the relative proportions of microglia sub-population with age in AD and NDC. We found that numbers of Micro3 nuclei, which most highly expressed apoptotic pathway genes, decreased with increasing age in the NDC brain tissues, as expected for a sub-population prone to apoptosis. However, this was not observed in AD, consistent with induction of senescence pathways and reduced apoptosis (Supplementary fig. 11a). To further validate this with an independent dataset, we integrated microglia nuclei from all the datasets used in the meta-analysis and used "transfer labelling" according to our subcluster annotation and found again that the proportion of Micro3 nuclei decreases with increasing age in NDC but not in AD samples (Supplementary fig. 11b, Supplementary data S11). This suggests, AD associated pathology can trigger senescence as a reversal of apoptosis phenotype.

To define specific mechanisms conferring vulnerability to senescence in microglia with AD, we explored differential gene expression in the Micro1, Micro2 and Micro3 sub-populations with AD relative to that in the NDC and with regression against β-amyloid load across all tissues studied, regardless of disease association. Our first level of analysis better defined mechanisms responsible for the induction of senescence. All three microglial sub-populations showed upregulation of *APOE, ATG16L2* (an autophagy antagonist gene), *BCL2* (encoding a negative regulator of apoptosis), the CDK7 regulator gene *CCNH* and *GAS7* (the growth arrest-specific protein 7 gene).

Genes for negative regulators of senescence such as *GRB2* and *NIBAN1* were downregulated with increasing β-amyloid [17, 21, 34, 55]. The Micro3 subpopulation increased *TAOK1* expression, the protein product of which is involved in mitotic G2 DNA damage checkpoint signaling and the expression of genes for the positive regulators of senescence OXR1 (Oxidation Resistance 1) and PELI1 [46, 81] (Supplementary data S12).

To further characterize associated gene expression pathways from which triggers for senescence induction could be inferred, we generated disease-related pseudo-time trajectories from the total set of control and AD nuclei. We set Micro1 as the start of the pseudo-time as it most highly expressed homeostatic markers such as *P2RY12* and *CX3CR1*. Homeostatic (Micro1) to GPNMB_EYA2/LPL_CD83 (Micro2) and CRM_CCL3 (Micro4) responses were found to be two independent activation routes mirroring the observations in a recent pre-print [47]. Micro3 branched into a third route of the trajectory (Fig. 7a). Our pseudo-time analysis identified genes that were differentially expressed along the pseudo-time trajectories. These genes were grouped into gene co-expression modules which characterized the transcriptomic identity of the microglial sub-populations along the trajectory. (Supplementary fig. 12a, Supplementary data S13). Functional pathways including “lamellipodium assembly”, “Fc-gamma receptor signaling pathway involved in phagocytosis” and “chemokine signalling pathway” (were enriched in the Module-3 and Module-4 genes that found predominantly in early-pseudotime suggesting early microglial activation in response to β-amyloid accumulation (Fig. 7b, c, Supplementary data S13). Module-5, which was highly expressed in mid-pseudotime, included GPNMB_EYA2 associated genes *GPNMB, PLA2G7, MYO1E, SLC1A3, CPM*, and *NPL* and pathways involving “regulation of macrophage derived foam cell differentiation”, “cellular response to low-density lipoprotein particle stimulus” and “positive regulation of inflammatory response” suggesting a β-amyloid associated pro-inflammatory and potentially harmful phenotype (Fig. 7c, Supplementary fig. 12a). We found that SERPINE1, a known senescence marker and SASP factor, was co-expressed with these genes in Module-5 [73]. Regression analyses showed that module-5 gene set correlated strongly with increasing β-amyloid (Supplementary fig. 12b, Supplementary data S14). This suggests that microglial pro-inflammatory activation and senescence phenotype are downstream of β-amyloid response. Module-10 also was highly expressed in

Micro2, which was enriched for “NF-kappa B signaling pathway”, “mTOR signaling pathway” and “cellular senescence” pathways (Fig. 7c, Supplementary fig. 12a, Supplementary data S13). Module-8, which also showed enrichment for cellular senescence pathways, was most highly expressed in Micro3 and in late-pseudotime (Supplementary fig. 12a). *ZFP36L2, ZFP36L1, ATM, CX3CR1* and *C3* were amongst the genes highly expressed in module-8 (Fig. 7d). ZFP36L2, *ZFP36L1* are associated with SASP and *ATM* is known to be the key driver of DNA-damage induced senescence [82]. The Micro3 sub-population also highly expressed module-7 genes such as *CD74, APOE, FTL* and *FTH*, reflecting functional activation for chemokine-mediate migration and an immunosuppressive or pathological immune “exhaustion” (dystrophic) phenotype with greater β-amyloid load (Supplementary data S13). The co-expression of microglial functional activation and DNA damage gene expression and senescence transcripts in Micro3 suggest that β-amyloid induced activation can increase pro-survival phenotype in an otherwise apoptotic cell. Together, these trajectory analyses support the hypothesis that the senescence phenotype in microglia is expressed as part of a microglial inflammatory activation response to β-amyloid.

Discussion

Although recent evidence has identified premature cell senescence in AD brains [59], we are not aware of a comprehensive characterization of which cell types are most affected, their relative numbers or the mechanisms responsible [5, 25, 35]. Here, we have used a combination of snRNA sequencing and imaging mass cytometry to characterize cell senescence in AD, describing cell types affected, the association between senescence and AD pathology and providing transcriptomic evidence for mechanisms of senescence. Our results demonstrate that there is a substantial burden of senescent cells in brain cortical grey matter with AD and that cell senescence signatures are most prevalent in microglia and associated with inflammatory activation and downregulation of genes related to β-amyloid phagocytosis. We also provide evidence that microglial senescence in AD is related to β-amyloid by showing greater proportions of senescent microglia near β-amyloid plaques and with greater β-amyloid load, particularly in the sub-population of microglia most enriched for homeostatic markers (Micro1) and DAM-associated genes (Micro2). Additional supportive evidence of β-amyloid induced senescence came from

demonstration of the TREM2 genotype dependence of the senescence signature (see also recent preclinical evidence presented in pre-print [56]). An intriguing aspect of our results is the observed lack of senescence in carriers of the TREM2-R47H variant. Contrary to expectations, this absence of senescence does not confer protective effects, as senescence may not be the predominant phenotype in microglia carrying R47H mutations. Instead, our data suggest that the overall pathology burden associated with R47H, particularly in the context of reduced microglial activation, may overshadow any potential neurotoxic effects attributed to senescent microglia. Our data additionally suggests mechanisms that DNA damage, mitochondrial dysfunction and ER stress associated with inflammatory activation together confer vulnerability to premature senescence in microglia with AD. These associations were supported by pseudo-time analyses that demonstrated the relationships of expression of these pathways with senescence along the inferred progression of microglia towards the alternative end states of apoptosis or senescence, expression of which may be related to the severity and chronicity of the stressors responsible [59].

Previous studies have highlighted senescence in multiple brain cell types in AD [3, 16, 32, 52, 80]. Most have focused on single or small numbers of markers of senescence, which likely accounts for some differences in conclusions that have been drawn. We employed multiplexed immunohistology and transcriptomics analyses of *post-mortem* human brains to assess senescence more comprehensively. This highlighted the complexity of profiling senescence-related cell phenotypes. For example, we found increased levels of *GLB1* protein expression [19, 75] in microglia, oligodendrocytes and astrocytes. However, as GLB1 expression alone cannot distinguish between senescent cells and cells with intrinsically high lysosomal content and is less associated to senescence in post-mitotic cells such as neurons, we also employed p16 and p21 as markers of an arrested cell cycle and γH2AX to detect DNA double-strand breaks (DSBs)[41, 52]. We found microglia to be the only cell type with significant increase in all markers in AD. Microglia, oligodendrocytes and astrocytes transcriptomes all showed enrichment for genes upregulated in an early senescence ("senescence initiators") pathway, but only microglia showed full expression of the full canonical senescence pathway (CSP) [16]. By this criterion, only microglia showed strong evidence for premature senescence with AD. Our data suggest mitochondrial

dysfunction and ER stress are common mechanisms driving the premature microglial senescence in AD, but does not directly implicate impaired autophagy, as suggested by a recent preclinical study [69]. However, this deserves further investigation as it may reflect limitations of the range of cell processes, we were able to interrogate. Also mitochondrial dysfunction can lead to ER stress through impaired autophagy [4].

While we identified Olig2^{+} cells expressing some senescence markers, joint use of transcriptomic data was able to more probably ascribe this senescence signature predominantly to oligodendrocytes rather than OPC, which had been implicated in an earlier preclinical study [80]. Oligodendroglial cells also increased expression of ER and related cell stress pathway transcriptomes with increasing β-amyloid load. We found only a smaller, more partial senescence response associated with DSB identified by γH2AX and DNA damage associated pathway expression in inhibitory neurons specifically. Dehkordi et al. previously concluded that excitatory neurons uniquely expressed a senescence signature based on relative enrichment of nuclear genes expressed with an eigengene reflecting a canonical senescence response [16]. Our different conclusion likely reflects the lower specificity of the eigengene approach relative to the simultaneous application of the multiple approaches here, but also could be influenced by differences between the brains sampled in two studies, differences in pathological features correlated (early β-amyloid pathology here vs later phospho-Tau pathology in the earlier paper) and relative weights of the marker gene expressed (i.e., use of CDKN2D in excitatory neurons[16]). In line with this, we found an apparent difference in senescence cell burden between allocortex (EC) and neocortex (MTG, SSC).

The strengths of our study were that we applied both immunohistological and transcriptomic analyses to identify cells expressing senescence markers with AD and that we included analyses of regions showing different levels of AD pathology in each brain. However, like all previous studies of AD, our analyses described markers associated with senescence rather than providing direct evidence of permanent growth arrest for the potentially replicating glia. Processes leading to senescence also evolve dynamically, as our results showing varying degrees of partial senescence phenotypes with pseudo-time imply. Describing a dynamic process using a cross-sectional sampling strategy can lead to strong biases in inferences particularly

regarding the proportion of end stage events. This could introduce bias particularly towards underestimates of the senescent cell burden. Cell senescence also is related to aging, as we showed for the non-diseased control brains. Our analysis of the contribution of aging to senescence in AD (either directly or through interactions) was limited by the low range of ages in the donor population. As aging is the strongest risk factor for AD, this deserves further study. Finally, the power to detect differentially expressed genes with AD or β-amyloid depends strongly on numbers of independent samples [62]. While 49 different brain blocks were characterized for our study, the three regions studied from each brain are not fully independent. This limits confidence particularly for single gene identifications. We mitigated this by replication of key observations with independent datasets, by highlighting results in agreement with prior studies that this work was extending and by analyses of gene sets, for which power should be substantially higher. Nonetheless, more work needs to be done to more confidently define specific genes whose expression appears to drive the pathology.

Preclinical studies using different models have suggested that senolytic treatments can reduce the abundance of senescent cells, disease-relevant pathology and cognitive deficits [8, 56, 80]. The extent to which cell senescence could contribute either to susceptibility to or the progression of human AD is important to answer fully in assessing the therapeutic potential of senolytics for this indication. Our study describes extensive cell stress associated with premature senescence in microglia in established AD. It additionally highlights that, by reducing phagocytic gene signatures in microglia in association with the induction of premature senescence, β-amyloid could reduce its own clearance and potentiate disease progression. Based on our observations, we hypothesise that microglia should be a primary focus for senolytic treatments in AD. They might be used synergistically with other strategies to enhance clearance of β-amyloid pathology [11]. This therapeutic opportunity provides a rationale for further characterization of mechanisms responsible for premature senescence in microglia.

Methods

Brain tissue

This study was carried out in accordance with the Regional Ethics Committee and Imperial College Use of Human Tissue guidelines. Cases were selected based first on neuropathological diagnosis from UK brain banks (London Neurodegeneration [King's College London] and Parkinson's UK [Imperial College London] Brain Bank). We then excluded cases with clinical or pathological evidence for small vessel disease, stroke, cerebral amyloid angiopathy, diabetes, Lewy body pathology (TDP-43), or other neurological diseases. Where the information was available, cases were selected with a post-mortem delay of less than 60 h **(Supplementary file 1, 2)**. Cohort-1 included MTG cortical tissue from 10 donors (Braak stage 0–II) without evidence of clinically significant brain disease (non-diseased controls, NDC) and 10 neuropathologically defined AD (Braak stage V–VI)) donors (**Supplementary file 1**). Cohort-2 included EC, MTG and SSC cortices from a final set of 17 cases including 8 NDC donors (Braak stage 0–II) and 9 neuropathologically defined AD (Braak stage III–VI) donors (total of 49 brain samples) **(Extended Method Fig. 1, Supplementary file 2)**. Cortical samples from three regions were prepared from each brain to characterise pathology and transcript expression.

Immunohistochemistry (IHC)

IHC (**Table-1**) was performed on FFPE sections (n=49) from the EC, MTG and SSC of each brain studied and paired with material from the cryopreserved contralateral hemisphere used for nuclear preparations for snRNA sequencing. Standard immunostaining procedures as recommended by the manufacturer were followed using the ImmPRESS Polymer (Vector Laboratories) and Super Sensitive Polymer-HRP (Biogenex) kits. Briefly, after dewaxing and rehydration of slides, endogenous peroxidase activity was blocked with 0.3% H_2O_2, followed by antigen retrieval. For immunostaining using ImmPRESS kits, non-specific binding was blocked using 10% normal horse serum. Primary antibodies were incubated overnight at 4 °C. Species-specific ImmPRESS or Super Sensitive kits and DAB were used for antibody visualisation. Tissue was counter-stained by incubation in Mayer's haematoxylin (TCS Biosciences) for 2 min, followed by dehydration, clearing and mounting.

Image Analysis

Digital images were generated from IHC stained slides scanned using a Leica Aperio AT2 Brightfield Scanner (Leica Biosystems). Images were analysed using Halo software (Indica Labs) after optimisation of Indica Labs macros. Data from all cortical regions in each brain were combined.

Imaging Mass Cytometry (IMC)

FFPE 5-10µm sections were immunostained using lanthanide tagged antibodies before ablation. The slides underwent routine dewaxing and rehydration before undergoing antigen retrieval, in a pH8 Ethylenediaminetetraacetic acid (EDTA) buffer. The slides were then treated with a 10% normal horse serum (Vector Laboratories) blocking solution before incubation with an antibody cocktail at 4ºC overnight. The slides were washed in 0.02% Triton X-100 (Sigma-Aldrich) before incubation with the Iridium-intercalator (Fluidigm) then washed and air-dried. All antibody conjugation was performed using the Maxpar X8 protocol (Fluidigm).

IMC was performed using a Hyperion Tissue Imager (Standard BioTools, San Francisco, USA) coupled to a Helios mass cytometer. The instrument was first tuned using the manufacturer's 3-Element Full Coverage Tuning Slide before the slides were loaded into the device. Four 500x500µm^2 regions of interest (ROI) within the grey matter were selected and ablated using a laser operating at a frequency of 200Hz with 1µm resolution. The data was stored as .mcd files compatible with MCD Viewer software (Fluidigm) and exported as TIFF files.

Co-localisation of IMC markers for Cohort-1

For the first IMC experiment (Cohort-1, Fig. 1a, b), the panel included antibodies listed in **Table-2**. The IMC channels which define a cell type were selected for masking, namely Iba1, GFAP, OLIG2, GLUT1, and MAP2. ImageJ (1.53c) was used for threshold correction and the despeckle function to reduce background noise. All of these channels were merged into a single field, alongside a DNA channel. The DNA channel was rendered red, while the cell type channels were rendered green before being saved as a JPEG. This JPEG was then used in Ilastik (1.1.3post3) using the pixel classification tool, this was then used to create a probability map clearly defining the images nuclei, cell signal and background. Finally, this probability map was

imported to CellProfiler (4.2.1) for masking. Once masked the sample was opened in HistoCAT (1.76) and the masked cell data was exported as a csv, with quantitative values for the signal of each IMC channel for each cell.

For peri-plaque microglia calculation (Fig. 4a, b, S1), the IMC channels Iba1, 4G8, p16 and GLB1 were saved as individual JPEGs for each sample using the ImageJ (1.53c) software, these images were then imported to Ilastik (1.1.3post3) were the cell signal and background were clearly identified as probability maps. These probability maps were then imported into CellProfiler (4.2.1). Each image was masked to identify cell signal as primary objects. The 4G8 primary objects were dilated by 10µm to encompass any high proximity microglia. The Iba1, p16 and GLB1 objects were then merged, keeping only overlapping objects to identify either $p16^+$, $GLB1^+$ or $p16^+GLB1^+$ positive microglia, the masked cell data was exported as a csv, with quantitative values for the signal of each IMC channel for each cell.

Automated IMC image analysis for Cohort-2

For the first IMC experiment (Cohort-1, Fig. 1c-e, S2, S11), the panel included antibodies listed in **Table-3**. The SIMPLI[7] pipeline (v. 1.1.0) was used for automated image processing and analysis for cohort-2 (4 ROI per section taken from 49 different brain blocks resulting in 194 QC-passed ROIs). This includes image processing (extraction of single .txt files from each ROI to TIFF images), normalisation and pre-processing using CellProfiler, where threshold smoothing scale, correction factor, lower and upper bounds, and manual threshold in were adjusted for each channel to remove background and keep specific signal only. Single-nuclei segmentation was performed within SIMPLI based on the intercalator (191Ir/193Ir) channel using StarDist, with the “2D_versatile_fluo” model and a probability threshold of 0.05. Single-nuclei channels intensity was used by SIMPLI for masking all detected nuclei to identify those expressing at least one of the cell type markers used (Iba1, OLIG2, MAP2, GFAP, GLUT1). Seurat, included in SIMPLI, was then used for unsupervised clustering of the identified cells (resolution 0.8). Resulting clusters were assigned to cell types based on cell type markers expression: 4 GLUT1+ clusters were assigned to endothelial cells (cluster 0, 11, 13, 14), 2 Iba1+ clusters to microglia (cluster 1, 9), 4 OLIG2+ clusters to oligodendrocytes (cluster 2, 3, 6, 12), 1 GFAP+ cluster to astrocytes (cluster 7) and 4 MAP2+ clusters to neurons (cluster 4, 5, 8, 10). Cluster

that expressed more than one marker were excluded from downstream analysis (cluster 10, 12, 14) with the exception of cluster7 which was the only cluster expressing GFAP.

Calculation of senescent nuclei in IMC for Cohort-2

First, mean senescence marker (GLB1, p16, p21, γ-H2AX) expression was calculated per ROI and ROIs with the lowest 1% expression were excluded. Cells with the lowest 1% cell marker (Iba1, GFAP, MAP2, OLIG2, GLUT1) expression were removed from each ROI. The number of cells were then summed up across the ROIs at the sample level. The final numbers of ROIs per sample ranged between 3-4. Samples with < 3 cells per cluster were removed from subsequent analysis. Proportion of senescent nuclei per sample was then calculated by taking the ratio of cells co-expressing cell and senescence markers to cells positive for cell markers only. A Wilcoxon rank-sum test was performed to compare the differences of senescent nuclei proportion between AD and NDC across all clusters stratified by brain region and the effect sizes was calculated by the rank-biserial correlation[37]. The Wilcoxon rank-sum test was performed by wilcox.test() function, the p-value and the 95% confidence intervals were calculated by rank_biserial() function from effectsize (v. 0.8.6) package in R.

Single nucleus isolation

Single nucleus isolation was conducted on 49 tissue blocks from (*n*=24, NDC; *n*=25, AD). Two samples were not available for sample preparation. Homologous fresh frozen brain tissue blocks from the EC, MTG and SSC were cryosectioned at 80um and 200mg of grey matter was collected in RNAse-free Eppendorf tube, as previously described [66]. Nuclei were isolated as previously described[66] using a protocol based on [40]. All steps were carried out on ice or at 4°C. Tissue was homogenised in buffer (1% Triton X-100, 0.4 U/µl RNAseIn + 0.2 U/µl SUPERaseIn, 1ul 1mg/ml DAPI) using a 2ml glass douncer. The homogenate was centrifuged at 4°C for 8mins, 500g and supernatant removed. The pellet then was resuspended in homogenisation buffer and filtered through a 70um filter followed by density gradient centrifugation at 13,000g for 40mins. The supernatant was removed and nuclei were washed and filtered in PBS buffer (PBS + 0.5mg/ml BSA + 0.4 U/µl RNAseIn + 0.2 U/µl SUPERaseIn). Nuclei were pelleted, washed twice in PBS buffer and resuspended in 1ml PBS buffer. 100ul of nuclei solution was set aside on ice for single nuclear processing.

Single nucleus processing and sequencing

Isolated nuclei stained with Acridine Orange dye were counted on a LUNA-FL Dual Fluorescence Cell Counter (Logos Biosystems, L20001). Approximately 7000 nuclei were used for 10x Genomics Chromium Single Cell 3' processing and library generation. All steps were conducted according to the 10x Genomics Chromium Single Cell 3' Reagent Kits v3 User Guide, with 8 cycles of cDNA amplification until fragmentation, where 25ng of amplified cDNA per sample was taken through for fragmentation. The final index PCR was conducted at 14 cycles. cDNA and library prep concentration were measured using Qubit dsDNA HS Assay Kit (ThermoFisher, Q32851) and DNA and library preparations were assessed using the Bioanalyzer High-Sensitivity DNA Kit (Agilent, 5067-4627). Pooled samples at equimolar concentrations were sequenced on an Illumina HiSeq 4000 according to the standard 10X Genomics protocol.

Pre-processing and quality-control of snRNA sequencing data

Alignment and demultiplexing of raw sequencing data was performed using 10X Genomics Cell Ranger v3.1, with a pre-mRNA GRCh38 genome reference including both introns and exons. Downstream primary analyses of gene-cell matrices were performed using our scFlow pipeline [38]. Ambient RNA profiling was performed using emptyDrops with a lower parameter of <100 counts, an alpha cutoff of ≤0.001, and with 10,000 Monte-Carlo iterations [45]. Cells containing ≥200 total counts or total expressive features, where expressivity was defined as a minimum of 2 counts in at least 3 cells, were included. An adaptive threshold was used to exclude nuclei with more than 4 median absolute deviation (MAD) total counts or total expressive features within a sample. The maximum proportion of counts mapping to mitochondrial genes was set to 5%. Doublets were identified using the DoubletFinder algorithm, with a doublets-per-thousand-cells increment of 8 cells (recommended by 10X Genomics), a pK value of 0.005, and embeddings were generated using the first ten principal components calculated from the top 2000 most highly variable genes (HVGs) [50].

Integration, clustering, and visualization of data

The linked inference of genomic experimental relationships (LIGER) package was used to calculate integrative factors across samples [77]. LIGER parameters used included: k: 20, lambda: 5.0, thresh: 0.0001, max_iters: 100, knn_k: 20, min_cells: 2,

quantiles: 50, nstart: 10, resolution: 1, num_genes: 3000, center: false. Two-dimensional embeddings of the LIGER integrated factors were calculated using the uniform-manifold approximation and projection (UMAP) algorithm with the following parameters: pca_dims: 30, n_neighbours: 70, init: spectral, metric: euclidean, n_epochs: 200, learning_rate: 1, min_dist: 0.7, spread: 0.85, set_op_mix_ratio: 1, local connectivity: 1, repulsion_strength: 1, negative_sample_rate: 5, fast_sgd: false (McInnes et al., 2018). The Leiden community detection algorithm was used to detect clusters of cells from the 2D UMAP (LIGER) embeddings; a resolution parameter of 0.0001 and a k value of 40 was used [70].

Assigning cell type labels to snRNAseq cells

Automated cell-typing was performed essentially as previously described using the Expression Weighted Celltype Enrichment (EWCE) algorithm in scFlow against a previously generated cell-type data reference from the Allan Human Brain Atlas [38, 65]. The top five marker genes for each automatically annotated cell-type were determined using Monocle 3 and validated against canonical cell-type markers [71].

Differential gene expression analysis

We used model-based analysis of single-cell transcriptomics (MAST) to identify genes differentially expressed (associated) between AD and NDC and with histopathological features (using 4G8 amyloid), using each feature as a dependent variable in a zero-inflated regression analysis using a mixed-model [20]. Data from both regions was combined. Additionally, diagnosis (control, AD) was used as a dependent variable to identify DGE between experimental groups. Models were fit separately for each cell-type. The model specification was zlm(~dependent_variable + (1|sample) + cngeneson + pc_mito + sex + brain_region + age + PMI, method = “glmer”, ebayes = F). The fixed-effect term cngeneson is the cellular detection rate as previously described, and pc_mito accounts for the relative proportion of counts mapping to mitochondrial genes. Each model was fit with and without the dependent variable and compared using a likelihood ratio test. Genes expressed in at least 10% of cells (minimum of 2 counts per cell) were evaluated for gene expression. The threshold for significant differential gene expression was a log2 fold-change of at least 0.25 and an adjusted p-value < 0.05.

Impacted pathway analysis

Impacted pathway analysis (IPA) was performed essentially as previously described using the enrichR packages in scFlow [12, 44]. Statistically significant differentially expressed genes were submitted for IPA with the over-representation analysis (ORA) enrichment method against the 'GO_Biological_Process' and 'KEGG' databases. The false-discovery rate (FDR) was calculated using the Benjamini-Hochberg method and filtering was applied at a significance threshold of ≤0.05.

Gene set score visualisation

Dot plot (Fig. 2c) was generated using Seurat DotPlot() function using CSP, SIP and custom list (Supplementary data S5). Genes expressed in less than 10% of any cell population were excluded. Gene set or module featureplots were generated by first calculating aggregated gene set scores using AddModuleScore() function from Seurat and then plotted using FeaturePlot scCustom() from scCustomize (v. 2.0.1).

Gene set enrichment analyses (GSEA)

Gene sets were collected either from published literature or from publicly available databases. "canonical senescence pathway", "senescence initiating pathway" and "senescence response pathway" was collected from [16]. A custom set of senescence genes were used in Fig. 2c and S3a. Additional pathways were selected from Gene Ontology (GO) and KEGG databases using the search terms "senescence", "endoplasmic reticulum stress", "endosome", "endosomal", "lysosome", "lysosomal", "mitochondrial" and "oxidative stress". Pathways with less than 10 genes were excluded. Pathways that included positive or negative regulation in the description also were excluded from the resultant term list, yielding 33 biological processes (Supplementary data S5). We then used AUCell (R package v1.6.1) to quantify the expression of the gene set signature in each nucleus. Normalised data were processed in AUCell using the AUCell_build. Rankings function to generate ranking of each gene. The resulting rankings, along with the gene lists of interest, were then run by the function AUCell_calcAUC (aucMaxRank set to 5% of the number of input genes) to generate AUC scores of the gene in each nucleus. We then used the dream function from variancePartition package in R [31] to compare the expression changes across the categorical variables or regressed against β-amyloid densities. We used a linear mixed-model where individual sample "manifest" were set as the random effect

to avoid the pseudoreplication bias and the following covariates (total_features_by_counts, pc_mito, sex, brain_region, age and PMI) were set as fixed effects.

Quantification of senescent nuclei fraction using gene set score

Gene set scores for the “canonical senescence pathway (CSP)” was calculated per nucleus as described in the previous section. Cells were considered senescent if the gene set score was >median + 3 MADs (median absolute deviation).

Meta-analysis

Publicly available snRNA sequencing data (Supplementary data S8) were downloaded with appropriate authorization where required. Individual datasets were processed uniformly with similar parameters using nf-core/scflow as described above. For meta-analysis, microglial clusters were isolated, “canonical senescence pathway” gene set scores were calculated per nuclei as described above. Gene set scores were then averaged across all the nuclei per sample and meta-analysis was performed using the runMetaAnalysis() function from R package MetaIntegrator (v. 2.1.3). Meta-analysis result was visualised as a forest plot generated from R package forestplot (v. 3.1.1).

Sub-clustering and annotation

We generated transcriptomically-defined subsets for each of the glial cell type clusters (astrocytes, microglia and oligodendrocytes). To do this, individual cell type clusters were first normalized and scaled using Seurat’s NormalizeData and ScaleData functions respectively. RunPCA function was used to calculate the first 20 PCs using the top 2000 highly variable genes. Individual samples were re-integrated using Harmony [39], using Seurat’s RunHarmony() function (group.by.vars = "manifest"). To produce the final UMAP, we used the following parameters in RunUMAP() (dims = 1:20, n.epochs = 200). To identify clusters, we used first the function FindNeighbors() (dims = 1:20) and then performed unbiased clustering by using FindClusters() (resolution = 0.5). To annotate the sub-population of microglia, we used the gene sets from [47].

Pseudo-time

Pseudo-time analysis was performed to infer the phenotypic transitions happening between the different sub-population of each glial cell types. Unsupervised single-cell trajectory analysis was performed with *Monocle3*, an algorithm that allows to learn the sequence of gene expression changes each cell must go through as part of a dynamic biological process. We used *SeuratWrappers* to convert our *Seurat* object into a *Monocle* object with *as.cell_data_set()*. We kept the UMAP embeddings previously calculated with *RunUMAP()* in order to estimate the phenotypic transitions between our annotated cell states. We run *cluster_cells()* and *learn_graph()* (resolution = 0.001, use_partition = F, *close_loop = F, learn_graph_control = list(rann.k=100, prune_graph = TRUE, orthogonal_proj_tip = F, minimal_branch_len = 10, ncenter = 300)*) to learn the trajectory.

Acknowledgements

We thank the donors and their families for the human brain tissue in this study and UK brain bank staff for making it available. Tissue samples were provided by the London Neurodegenerative Diseases Brain Bank at King's College London, which receives funding from the UK Medical Research Council and from the Brains for Dementia Research programme, jointly funded by Alzheimer's Research UK and the Alzheimer's Society. Tissue samples and associated clinical and neuropathological data also were supplied by Parkinson's UK Brain Bank at Imperial, funded by Parkinson's UK, a charity registered in England and Wales (258197) and in Scotland (SC037554). We are grateful to Diana Benitez for her support for the human tissue management.

Infrastructure, including particularly the LMS/NIHR Imperial Biomedical Research Centre Flow Cytometry Facility and the Imperial BRC Genomics Facility, was supported by the Imperial College Healthcare Trust National Institute for Health Research (NIHR) Biomedical Research Centre (BRC). ST was supported by an "Early Postdoc Mobility" scholarship (P2GEP3_191446) from the Swiss National Science Foundation and a "Clinical Medicine Plus" scholarship from the Prof Dr Max Cloëtta Foundation (Zurich, Switzerland). PMM acknowledges generous personal support from the Edmond J Safra Foundation and Lily Safra and an NIHR Senior Investigator Award. This work was supported by the UK Dementia Research Institute, which receives its funding from UK DRI Ltd., funded by the UK Medical Research Council,

Alzheimer's Society, and Alzheimer's Research UK. The study is an output from the UK Dementia Institute Multi-omics Atlas Project for Alzheimer's Disease (MAP-AD; map-ad.org).

Declarations

This study also was partly funded by Biogen IDEC. PMM has received consultancy fees from Sudo Biosciences, Ipsen Biopharm Ltd., Rejuveron Therapeutics and Biogen. He has received honoraria or speakers' fees from Novartis and Biogen and has received research or educational funds from BMS, Biogen, Novartis and GlaxoSmithKline.

Data availability

The snRNAseq data will be made available to researchers for download from the Gene Expression Omnibus (GEO) database (https://www.ncbi.nlm.nih.gov/geo/) upon publication.

Code availability

All codes will be uploaded on github upon publication.

References

1. Askew K, Li K, Olmos-Alonso A, Garcia-Moreno F, Liang Y, Richardson P, Tipton T, Chapman MA, Riecken K, Beccari S, Sierra A, Molnár Z, Cragg MS, Garaschuk O, Perry VH, Gomez-Nicola D (2017) Coupled Proliferation and Apoptosis Maintain the Rapid Turnover of Microglia in the Adult Brain. Cell Rep 18:391. doi: 10.1016/J.CELREP.2016.12.041
2. Bernadotte A, Mikhelson VM, Spivak IM (2016) Markers of cellular senescence. Telomere shortening as a marker of cellular senescence. Aging (Albany NY) 8:3. doi: 10.18632/AGING.100871
3. Bhat R, Crowe EP, Bitto A, Moh M, Katsetos CD, Garcia FU, Johnson FB, Trojanowski JQ, Sell C, Torres C (2012) Astrocyte senescence as a component of Alzheimer's disease. PLoS One 7:e45069–e45069. doi: 10.1371/journal.pone.0045069
4. Biczo G, Vegh ET, Shalbueva N, Mareninova OA, Elperin J, Lotshaw E, Gretler S, Lugea A, Malla SR, Dawson D, Ruchala P, Whitelegge J, French

SW, Wen L, Husain SZ, Gorelick FS, Hegyi P, Rakonczay Z, Gukovsky I, Gukovskaya AS (2018) Mitochondrial Dysfunction, Through Impaired Autophagy, Leads to Endoplasmic Reticulum Stress, Deregulated Lipid Metabolism, and Pancreatitis in Animal Models. Gastroenterology 154:689–703. doi: 10.1053/J.GASTRO.2017.10.012

5. Bielak-Zmijewska A, Wnuk M, Przybylska D, Grabowska W, Lewinska A, Alster O, Korwek Z, Cmoch A, Myszka A, Pikula S, Mosieniak G, Sikora E (2014) A comparison of replicative senescence and doxorubicin-induced premature senescence of vascular smooth muscle cells isolated from human aorta. Biogerontology 15:47–64. doi: 10.1007/s10522-013-9477-9

6. Blazek D, Kohoutek J, Bartholomeeusen K, Johansen E, Hulinkova P, Luo Z, Cimermancic P, Ule J, Peterlin BM (2011) The Cyclin K/Cdk12 complex maintains genomic stability via regulation of expression of DNA damage response genes. Genes Dev 25:2158–2172. doi: 10.1101/GAD.16962311

7. Bortolomeazzi M, Montorsi L, Temelkovski D, Keddar MR, Acha-Sagredo A, Pitcher MJ, Basso G, Laghi L, Rodriguez-Justo M, Spencer J, Ciccarelli FD (2022) A SIMPLI (Single-cell Identification from MultiPLexed Images) approach for spatially-resolved tissue phenotyping at single-cell resolution. Nat Commun 2022 131 13:1–14. doi: 10.1038/s41467-022-28470-x

8. Bussian TJ, Aziz A, Meyer CF, Swenson BL, van Deursen JM, Baker DJ (2018) Clearance of senescent glial cells prevents tau-dependent pathology and cognitive decline. Nature 562:578. doi: 10.1038/S41586-018-0543-Y

9. Butterfield DA, Swomley AM, Sultana R (2013) Amyloid β-peptide (1-42)-induced oxidative stress in Alzheimer disease: importance in disease pathogenesis and progression. Antioxid Redox Signal 19:823–835. doi: 10.1089/ARS.2012.5027

10. Caldeira C, Cunha C, Vaz AR, Falcão AS, Barateiro A, Seixas E, Fernandes A, Brites D (2017) Key aging-associated alterations in primary microglia response to beta-amyloid stimulation. Front Aging Neurosci 9. doi: 10.3389/FNAGI.2017.00277/FULL

11. CH van D, CJ S, P A, RJ B, C C, M G, M K, D L, L R, S C, L F, S K, M S, B V, D W, S D, M I, LD K, T I (2023) Lecanemab in Early Alzheimer's Disease. N Engl J Med 388:142–143. doi: 10.1056/NEJMOA2212948

12. Chen EY, Tan CM, Kou Y, Duan Q, Wang Z, Meirelles G V., Clark NR,

Ma’ayan A (2013) Enrichr: interactive and collaborative HTML5 gene list enrichment analysis tool. BMC Bioinformatics 14:128. doi: 10.1186/1471-2105-14-128

13. Childs BG, Baker DJ, Kirkland JL, Campisi J, Deursen JM van (2014) Senescence and apoptosis: dueling or complementary cell fates? EMBO Rep 15:1139. doi: 10.15252/EMBR.201439245

14. Coppé J-P, Desprez P-Y, Krtolica A, Campisi J (2010) The Senescence-Associated Secretory Phenotype: The Dark Side of Tumor Suppression. Annu Rev Pathol 8:99–118. doi: 10.1146/annurev-pathol-121808-102144.The

15. Debacq-Chainiaux F, Ben Ameur R, Bauwens E, Dumortier E, Toutfaire M, Toussaint O (2016) Stress-Induced (Premature) Senescence. 243–262. doi: 10.1007/978-3-319-26239-0_13

16. Dehkordi SK, Walker J, Sah E, Bennett E, Atrian F, Frost B, Woost B, Bennett RE, Orr TC, Zhou Y, Andhey PS, Colonna M, Sudmant PH, Xu P, Wang M, Zhang B, Zare H, Orr ME (2021) Profiling senescent cells in human brains reveals neurons with CDKN2D/p19 and tau neuropathology. Nat Aging 1:1107–1116. doi: 10.1038/s43587-021-00142-3

17. Diana P, Carvalheira GMG (2022) NIBAN1, Exploring its Roles in Cell Survival Under Stress Context. Front Cell Dev Biol 10. doi: 10.3389/FCELL.2022.867003

18. Dileep V, Boix CA, Mathys H, Marco A, Welch GM, Meharena HS, Loon A, Jeloka R, Peng Z, Bennett DA, Kellis M, Tsai LH (2023) Neuronal DNA double-strand breaks lead to genome structural variations and 3D genome disruption in neurodegeneration. Cell 186:4404-4421.e20. doi: 10.1016/J.CELL.2023.08.038

19. Dimri GP, Lee X, Basile G, Acosta M, Scott G, Roskelley C, Medrano EE, Linskens M, Rubelj I, Pereira-Smith O, et al. (1995) A biomarker that identifies senescent human cells in culture and in aging skin in vivo. Proc Natl Acad Sci U S A 92:9363–9367. doi: 10.1073/pnas.92.20.9363

20. Finak G, McDavid A, Yajima M, Deng J, Gersuk V, Shalek AK, Slichter CK, Miller HW, McElrath MJ, Prlic M, Linsley PS, Gottardo R (2015) MAST: a flexible statistical framework for assessing transcriptional changes and characterizing heterogeneity in single-cell RNA sequencing data. Genome Biol 16. doi: 10.1186/S13059-015-0844-5

21. Fisher RP, Morgan DO (1994) A novel cyclin associates with M015/CDK7 to form the CDK-activating kinase. Cell 78:713–724. doi: 10.1016/0092-8674(94)90535-5
22. Fonseka CY, Rao DA, Teslovich NC, Korsunsky I, Hannes SK, Slowikowski K, Gurish MF, Donlin LT, Lederer JA, Weinblatt ME, Massarotti EM, Coblyn JS, Helfgott SM, Todd DJ, Bykerk VP, Karlson EW, Ermann J, Lee YC, Brenner MB, Raychaudhuri S (2018) Mixed-effects association of single cells identifies an expanded effector CD4+ T cell subset in rheumatoid arthritis. Sci Transl Med 10. doi: 10.1126/SCITRANSLMED.AAQ0305
23. Gazestani V, Kamath T, Nadaf NM, Dougalis A, Burris SJ, Rooney B, Junkkari A, Vanderburg C, Pelkonen A, Gomez-Budia M, Välimäki NN, Rauramaa T, Therrien M, Koivisto AM, Tegtmeyer M, Herukka SK, Abdulraouf A, Marsh SE, Hiltunen M, Nehme R, Malm T, Stevens B, Leinonen V, Macosko EZ (2023) Early Alzheimer's disease pathology in human cortex involves transient cell states. Cell 186:4438-4453.e23. doi: 10.1016/J.CELL.2023.08.005
24. González-Gualda E, Baker AG, Fruk L, Muñoz-Espín D (2021) A guide to assessing cellular senescence in vitro and in vivo. FEBS J 288:56–80. doi: 10.1111/FEBS.15570
25. Gorgoulis V, Adams PD, Alimonti A, Bennett DC, Bischof O, Bishop C, Campisi J, Collado M, Evangelou K, Ferbeyre G, Gil J, Hara E, Krizhanovsky V, Jurk D, Maier AB, Narita M, Niedernhofer L, Passos JF, Robbins PD, Schmitt CA, Sedivy J, Vougas K, von Zglinicki T, Zhou D, Serrano M, Demaria M (2019) Cellular Senescence: Defining a Path Forward. Cell 179:813–827. doi: https://doi.org/10.1016/j.cell.2019.10.005
26. Guerreiro R, Bras J (2015) The age factor in Alzheimer's disease. Genome Med 7:106. doi: 10.1186/s13073-015-0232-5
27. Guerrero A, De Strooper B, Arancibia-Cárcamo IL (2021) Cellular senescence at the crossroads of inflammation and Alzheimer's disease. Trends Neurosci 44:714–727. doi: https://doi.org/10.1016/j.tins.2021.06.007
28. Hayflick L, Moorhead PS (1961) The serial cultivation of human diploid cell strains. Exp Cell Res 25:585–621. doi: https://doi.org/10.1016/0014-4827(61)90192-6
29. Herdy JR, Traxler L, Agarwal RK, Karbacher L, Schlachetzki JCM, Boehnke L, Zangwill D, Galasko D, Glass CK, Mertens J, Gage FH (2022) Increased post-

mitotic senescence in aged human neurons is a pathological feature of Alzheimer's disease. Cell Stem Cell 29:1637-1652.e6. doi: 10.1016/J.STEM.2022.11.010

30. Higgs MR, Reynolds JJ, Winczura A, Blackford AN, Borel V, Miller ES, Zlatanou A, Nieminuszczy J, Ryan EL, Davies NJ, Stankovic T, Boulton SJ, Niedzwiedz W, Stewart GS (2015) BOD1L Is Required to Suppress Deleterious Resection of Stressed Replication Forks. Mol Cell 59:462–477. doi: 10.1016/J.MOLCEL.2015.06.007

31. Hoffman GE, Schadt EE (2016) variancePartition: Interpreting drivers of variation in complex gene expression studies. BMC Bioinformatics 17:1–13. doi: 10.1186/S12859-016-1323-Z/FIGURES/5

32. Hu Y, Fryatt GL, Ghorbani M, Obst J, Menassa DA, Martin-Estebane M, Muntslag TAO, Olmos-Alonso A, Guerrero-Carrasco M, Thomas D, Cragg MS, Gomez-Nicola D (2021) Replicative senescence dictates the emergence of disease-associated microglia and contributes to Aβ pathology. Cell Rep 35:109228. doi: https://doi.org/10.1016/j.celrep.2021.109228

33. Jäkel S, Agirre E, Mendanha Falcão A, van Bruggen D, Lee KW, Knuesel I, Malhotra D, ffrench-Constant C, Williams A, Castelo-Branco G (2019) Altered human oligodendrocyte heterogeneity in multiple sclerosis. Nat 2019 5667745 566:543–547. doi: 10.1038/s41586-019-0903-2

34. Jiang W, Wei K, Pan C, Li H, Cao J, Han X, Tang Y, Zhu S, Yuan W, He Y, Xia Y, Chen L, Chen Y (2018) MicroRNA-1258 suppresses tumour progression via GRB2/Ras/Erk pathway in non-small-cell lung cancer. Cell Prolif 51. doi: 10.1111/CPR.12502

35. Jurk D, Wang C, Miwa S, Maddick M, Korolchuk V, Tsolou A, Gonos ES, Thrasivoulou C, Jill Saffrey M, Cameron K, von Zglinicki T (2012) Postmitotic neurons develop a p21-dependent senescence-like phenotype driven by a DNA damage response. Aging Cell 11:996–1004. doi: https://doi.org/10.1111/j.1474-9726.2012.00870.x

36. Kelley KD, Miller KR, Todd A, Kelley AR, Tuttle R, Berberich SJ (2010) YPEL3, a p53-regulated gene that induces cellular senescence. Cancer Res 70:3566–3575. doi: 10.1158/0008-5472.CAN-09-3219

37. Kerby DS (2014) The Simple Difference Formula: An Approach to Teaching Nonparametric Correlation1. http://dx.doi.org/102466/11IT31 3:11.IT.3.1. doi:

10.2466/11.IT.3.1
38. Khozoie C, Fancy N, Marjaneh MM, Murphy AE, Matthews PM, Skene N (2021) scFlow: A Scalable and Reproducible Analysis Pipeline for Single-Cell RNA Sequencing Data. bioRxiv 2021.08.16.456499. doi: 10.1101/2021.08.16.456499
39. Korsunsky I, Millard N, Fan J, Slowikowski K, Zhang F, Wei K, Baglaenko Y, Brenner M, Loh P ru, Raychaudhuri S (2019) Fast, sensitive and accurate integration of single-cell data with Harmony. Nat Methods 2019 1612 16:1289–1296. doi: 10.1038/s41592-019-0619-0
40. Krishnaswami SR, Grindberg R V., Novotny M, Venepally P, Lacar B, Bhutani K, Linker SB, Pham S, Erwin JA, Miller JA, Hodge R, McCarthy JK, Kelder M, McCorrison J, Aevermann BD, Fuertes FD, Scheuermann RH, Lee J, Lein ES, Schork N, McConnell MJ, Gage FH, Lasken RS (2016) Using single nuclei for RNA-seq to capture the transcriptome of postmortem neurons. Nat Protoc. doi: 10.1038/nprot.2016.015
41. Kuilman T, Michaloglou C, Mooi WJ, Peeper DS (2010) The essence of senescence. Genes Dev 24:2463–2479. doi: 10.1101/gad.1971610
42. Lee BY, Han JA, Im JS, Morrone A, Johung K, Goodwin EC, Kleijer WJ, DiMaio D, Hwang ES (2006) Senescence-associated β-galactosidase is lysosomal β-galactosidase. Aging Cell 5:187–195. doi: 10.1111/J.1474-9726.2006.00199.X
43. Levine J, Kwon E, Paez P, Yan W, Czerwieniec G, Loo JA, Sofroniew M V., Wanner IB (2016) Traumatically injured astrocytes release a proteomic signature modulated by STAT3 dependent cell survival. Glia 64:668. doi: 10.1002/GLIA.22953
44. Liao Y, Wang J, Jaehnig EJ, Shi Z, Zhang B (2019) WebGestalt 2019: gene set analysis toolkit with revamped UIs and APIs. Nucleic Acids Res 47:W199–W205. doi: 10.1093/NAR/GKZ401
45. Lun ATL, Riesenfeld S, Andrews T, Dao TP, Gomes T, Marioni JC (2019) EmptyDrops: distinguishing cells from empty droplets in droplet-based single-cell RNA sequencing data. Genome Biol 20. doi: 10.1186/S13059-019-1662-Y
46. Ma JH, Zhang YT, Wang LP, Sun QY, Zhang H, Li JJ, Han NN, Zhu YY, Xie XY, Li X (2022) K63 Ubiquitination of P21 Can Facilitate Pellino-1 in the Context of Chronic Obstructive Pulmonary Disease and Lung Cellular

Senescence. Cells 11:3115. doi: 10.3390/CELLS11193115/S1

47. Mancuso R, Fattorelli N, Martinez-Muriana A, Davis E, Wolfs L, Van J, Daele D, Geric I, Preman P, Serneels L, Poovathingal S, Balusu S, Verfaille C, Fiers M, De Strooper B (2022) A multi-pronged human microglia response to Alzheimer's disease Aβ pathology. bioRxiv 2022.07.07.499139. doi: 10.1101/2022.07.07.499139

48. Marques S, Zeisel A, Codeluppi S, Van Bruggen D, Falcão AM, Xiao L, Li H, Häring M, Hochgerner H, Romanov RA, Gyllborg D, Muñoz-Manchado AB, La Manno G, Lönnerberg P, Floriddia EM, Rezayee F, Ernfors P, Arenas E, Hjerling-Leffler J, Harkany T, Richardson WD, Linnarsson S, Castelo-Branco G (2016) Oligodendrocyte heterogeneity in the mouse juvenile and adult central nervous system. Science (80-) 352:1326–1329. doi: 10.1126/science.aaf6463

49. Matsudaira T, Nakano S, Konishi Y, Kawamoto S, Uemura K, Kondo T, Sakurai K, Ozawa T, Hikida T, Komine O, Yamanaka K, Fujita Y, Yamashita T, Matsumoto T, Hara E (2023) Cellular senescence in white matter microglia is induced during ageing in mice and exacerbates the neuroinflammatory phenotype. Commun Biol 2023 61 6:1–13. doi: 10.1038/s42003-023-05027-2

50. McInnes L, Healy J, Saul N, Großberger L (2018) UMAP: Uniform Manifold Approximation and Projection. J Open Source Softw 3:861. doi: 10.21105/JOSS.00861

51. Mirzayans R, Andrais B, Hansen G, Murray D (2012) Role of p16 INK4A in replicative senescence and DNA damage-induced premature senescence in p53-deficient human cells. Biochem Res Int. doi: 10.1155/2012/951574

52. Musi N, Valentine JM, Sickora KR, Baeuerle E, Thompson CS, Shen Q, Orr ME (2018) Tau protein aggregation is associated with cellular senescence in the brain. Aging Cell 17:12840. doi: 10.1111/ACEL.12840

53. Olah M, Patrick E, Villani A-C, Xu J, White CC, Ryan KJ, Piehowski P, Kapasi A, Nejad P, Cimpean M, Connor S, Yung CJ, Frangieh M, McHenry A, Elyaman W, Petyuk V, Schneider JA, Bennett DA, De Jager PL, Bradshaw EM (2018) A transcriptomic atlas of aged human microglia. Nat Commun 9:539. doi: 10.1038/s41467-018-02926-5

54. Osorio D, Cai JJ (2021) Systematic determination of the mitochondrial proportion in human and mice tissues for single-cell RNA-sequencing data quality control. Bioinformatics 37:963. doi:

10.1093/BIOINFORMATICS/BTAA751

55. Paglinawan R, Malipiero U, Schlapbach R, Frei K, Reith W, Fontana A (2003) TGFβ directs gene expression of activated microglia to an anti-inflammatory phenotype strongly focusing on chemokine genes and cell migratory genes. Glia 44:219–231. doi: 10.1002/GLIA.10286

56. Rachmian N, Medina S, Cherqui U, Akiva H, Deitch D, Edilbi D, Croese T, Salame T, Ramos JP, Cahalon L, Krizhanovsky V, Schwartz M (2023) TREM2-dependent senescent microglia conserved in aging and Alzheimer's disease. bioRxiv 2023.03.20.533401. doi: 10.1101/2023.03.20.533401

57. Rawji KS, Mishra MK, Michaels NJ, Rivest S, Stys PK, Yong VW (2016) Immunosenescence of microglia and macrophages: impact on the ageing central nervous system. Brain 139:653. doi: 10.1093/BRAIN/AWV395

58. Sadick JS, O'Dea MR, Hasel P, Dykstra T, Faustin A, Liddelow SA (2022) Astrocytes and oligodendrocytes undergo subtype-specific transcriptional changes in Alzheimer's disease. Neuron 110:1788-1805.e10. doi: 10.1016/J.NEURON.2022.03.008

59. Saez-Atienzar S, Masliah E (2020) Cellular senescence and Alzheimer disease: the egg and the chicken scenario. Nat Rev Neurosci 21:433–444. doi: 10.1038/s41583-020-0325-z

60. Sala Frigerio C, Wolfs L, Fattorelli N, Thrupp N, Voytyuk I, Schmidt I, Mancuso R, Chen WT, Woodbury ME, Srivastava G, Moller T, Hudry E, Das S, Saido T, Karran E, Hyman B, Perry VH, Fiers M, De Strooper B (2019) The Major Risk Factors for Alzheimer's Disease: Age, Sex, and Genes Modulate the Microglia Response to Abeta Plaques. Cell Rep 27:1293-1306 e6. doi: 10.1016/j.celrep.2019.03.099

61. Saul D, Kosinsky RL, Atkinson EJ, Doolittle ML, Zhang X, LeBrasseur NK, Pignolo RJ, Robbins PD, Niedernhofer LJ, Ikeno Y, Jurk D, Passos JF, Hickson LTJ, Xue A, Monroe DG, Tchkonia T, Kirkland JL, Farr JN, Khosla S (2022) A new gene set identifies senescent cells and predicts senescence-associated pathways across tissues. Nat Commun 13. doi: 10.1038/S41467-022-32552-1

62. Schmid KT, Höllbacher B, Cruceanu C, Böttcher A, Lickert H, Binder EB, Theis FJ, Heinig M (2021) scPower accelerates and optimizes the design of multi-sample single cell transcriptomic studies. Nat Commun 2021 121 12:1–18. doi:

10.1038/s41467-021-26779-7
63. Serrano-Pozo A, Frosch MP, Masliah E, Hyman BT (2011) Neuropathological alterations in Alzheimer disease. Cold Spring Harb Perspect Med 1:a006189
64. Sharpe JC, Arnoult D, Youle RJ (2004) Control of mitochondrial permeability by Bcl-2 family members. Biochim Biophys Acta - Mol Cell Res 1644:107–113. doi: 10.1016/J.BBAMCR.2003.10.016
65. Skene NG, Grant SGN (2016) Identification of vulnerable cell types in major brain disorders using single cell transcriptomes and expression weighted cell type enrichment. Front Neurosci 10:16. doi: 10.3389/FNINS.2016.00016/BIBTEX
66. Smith AM, Davey K, Tsartsalis S, Khozoie C, Fancy N, Tang SS, Liaptsi E, Weinert M, McGarry A, Muirhead RCJ, Gentleman S, Owen DR, Matthews PM (2022) Diverse human astrocyte and microglial transcriptional responses to Alzheimer's pathology. Acta Neuropathol 143:75–91. doi: 10.1007/s00401-021-02372-6
67. Spiller F, Medina-Pritchard B, Abad MA, Wear MA, Molina O, Earnshaw WC, Jeyaprakash AA (2017) Molecular basis for Cdk1-regulated timing of Mis18 complex assembly and CENP-A deposition. EMBO Rep 18:894. doi: 10.15252/EMBR.201643564
68. Sudom A, Talreja S, Danao J, Bragg E, Kegel R, Min X, Richardson J, Zhang Z, Sharkov N, Marcora E, Thibault S, Bradley J, Wood S, Lim A-C, Chen H, Wang S, Foltz IN, Sambashivan S, Wang Z (2018) Molecular basis for the loss-of-function effects of the Alzheimer's disease–associated R47H variant of the immune receptor TREM2. J Biol Chem 293:12634. doi: 10.1074/JBC.RA118.002352
69. Suelves N, Saleki S, Ibrahim T, Palomares D, Moonen S, Koper MJ, Vrancx C, Vadukul DM, Papadopoulos N, Viceconte N, Claude E, Vandenberghe R, von Arnim CAF, Constantinescu SN, Thal DR, Decottignies A, Kienlen-Campard P (2023) Senescence-related impairment of autophagy induces toxic intraneuronal amyloid-β accumulation in a mouse model of amyloid pathology. Acta Neuropathol Commun 2023 111 11:1–26. doi: 10.1186/S40478-023-01578-X
70. Traag VA, Waltman L, van Eck NJ (2019) From Louvain to Leiden:

guaranteeing well-connected communities. Sci Reports 2019 91 9:1–12. doi: 10.1038/s41598-019-41695-z

71. Trapnell C, Cacchiarelli D, Grimsby J, Pokharel P, Li S, Morse M, Lennon NJ, Livak KJ, Mikkelsen TS, Rinn JL (2014) The dynamics and regulators of cell fate decisions are revealed by pseudotemporal ordering of single cells. Nat Biotechnol 2014 324 32:381–386. doi: 10.1038/nbt.2859

72. Valério-Gomes B, Guimarães DM, Szczupak D, Lent R (2018) The Absolute Number of Oligodendrocytes in the Adult Mouse Brain. Front Neuroanat 12. doi: 10.3389/fnana.2018.00090

73. Vaughan DE, Rai R, Khan SS, Eren M, Ghosh AK (2017) Plasminogen Activator Inhibitor-1 Is a Marker and a Mediator of Senescence. Arterioscler Thromb Vasc Biol 37:1446–1452. doi: 10.1161/ATVBAHA.117.309451

74. Venkataraman A V, Mansur A, Rizzo G, Bishop C, Lewis Y, Kocagoncu E, Lingford-Hughes A, Huiban M, Passchier J, Rowe JB, Tsukada H, Brooks DJ, Martarello L, Comley RA, Chen L, Schwarz AJ, Hargreaves R, Gunn RN, Rabiner EA, Matthews PM (2021) Widespread cell stress and mitochondrial dysfunction in early Alzheimer's Disease. medRxiv 2021.08.11.21261851. doi: 10.1101/2021.08.11.21261851

75. Wagner J, Damaschke N, Yang B, Truong M, Guenther C, McCormick J, Huang W, Jarrard D (2015) Overexpression of the Novel Senescence Marker β-Galactosidase (GLB1) in Prostate Cancer Predicts Reduced PSA Recurrence. PLoS One 10. doi: 10.1371/JOURNAL.PONE.0124366

76. Weidling I, Swerdlow RH (2019) Mitochondrial Dysfunction and Stress Responses in Alzheimer's Disease. Biology (Basel) 8:39. doi: 10.3390/biology8020039

77. Welch JD, Kozareva V, Ferreira A, Vanderburg C, Martin C, Macosko EZ (2019) Single-Cell Multi-omic Integration Compares and Contrasts Features of Brain Cell Identity. Cell 177:1873-1887.e17. doi: 10.1016/J.CELL.2019.05.006/ATTACHMENT/06F5E42B-9A6F-4D19-B1FC-9C7A825B704E/MMC2.XLSX

78. Wu R, Yan Y, Ma C, Chen H, Dong Z, Wang Y, Liu Y, Liu M, Yang L (2019) HMGB1 contributes to SASH1 methylation to attenuate astrocyte adhesion. Cell Death Dis 10. doi: 10.1038/S41419-019-1645-7

79. Yosef R, Pilpel N, Papismadov N, Gal H, Ovadya Y, Vadai E, Miller S, Porat Z,

Ben-Dor S, Krizhanovsky V (2017) p21 maintains senescent cell viability under persistent DNA damage response by restraining JNK and caspase signaling. EMBO J 36:2280–2295. doi: 10.15252/EMBJ.201695553

80. Zhang P, Kishimoto Y, Grammatikakis I, Gottimukkala K, Cutler RG, Zhang S, Abdelmohsen K, Bohr VA, Misra Sen J, Gorospe M, Mattson MP (2019) Senolytic therapy alleviates Aβ-associated oligodendrocyte progenitor cell senescence and cognitive deficits in an Alzheimer's disease model. Nat. Neurosci. 22:719–728

81. Zhang X, Zhang S, Liu X, Wang Y, Chang J, Zhang X, Mackintosh SG, Tackett AJ, He Y, Lv D, Laberge RM, Campisi J, Wang J, Zheng G, Zhou D (2018) Oxidation resistance 1 is a novel senolytic target. Aging Cell 17:12780. doi: 10.1111/ACEL.12780

82. Zhao J, Zhang L, Lu A, Han Y, Colangelo D, Bukata C, Scibetta A, Yousefzadeh MJ, Li X, Gurkar AU, McGowan SJ, Angelini L, O'Kelly R, Li H, Corbo L, Sano T, Nick H, Pola E, Pilla SPS, Ladiges WC, Vo N, Huard J, Niedernhofer LJ, Robbins PD (2020) ATM is a key driver of NF-κB-dependent DNA-damage-induced senescence, stem cell dysfunction and aging. Aging (Albany NY) 12:4688. doi: 10.18632/AGING.102863

83. Zhao Y, Wu X, Li X, Jiang LL, Gui X, Liu Y, Sun Y, Zhu B, Piña-Crespo JC, Zhang M, Zhang N, Chen X, Bu G, An Z, Huang TY, Xu H (2018) TREM2 Is a Receptor for β-Amyloid that Mediates Microglial Function. Neuron 97:1023-1031.e7. doi: 10.1016/J.NEURON.2018.01.031

Table 1: Antibodies used for Immunohistochemistry. *CB=citrate buffer. EDTA= ethylenediaminetetraacetic acid.*

Antibody	Supplier	Dilution	Antigen retrieval	Staining kit
β-Amyloid (4G8)	Biolegend, 800711	1:15,000	Steamer, CB pH6	Super Sensitive Polymer-HRP

Table 2: Antibodies used for imaging mass cytometry for Cohort-1.

Antibody	Gene name	Manufacturer	Catalouge	Metal-conjugate
β-amyloid (4G8)		Biolegend	800702	144 Nd
Iba1	AIF1	WAKO	019-19741	169 Tm
GFAP	GFAP	Abcam	ab218309	162 Dy
MAP2	MAP2	Abcam	ab236033	160 Gd
OLIG2	OLIG2	Abcam	ab220796	156 Gd
GLUT1	SLC2A1	Abcam	ab252403	176 Yb
p16	CDKN2A	Abcam	ab54210	141 Pr
GLB1	GLB1	Thermofisher	PA5-64417	161 Dy
DNA				191 Ir

Table 3: Antibodies used for imaging mass cytometry for Cohort-2.

Antibody	Gene name	Manufacturer	Catalouge	Metal-conjugate
β-amyloid (4G8)		Biolegend	800702	144 Nd
Iba1	AIF1	WAKO	019-19741	169 Tm
GFAP	GFAP	Abcam	ab218309	162 Dy
MAP2	MAP2	Abcam	ab236033	160 Gd

OLIG2	OLIG2	Abcam	ab220796	156 Gd
GLUT1	SLC2A1	Abcam	ab252403	176 Yb
p21	CDKN1A	Abcam	ab218311	158 Gd
p16	CDKN2A	Abcam	ab54210	141 Pr
GLB1	GLB1	Thermofisher	PA5-64417	161 Dy
yH2Ax	H2AX	Novus	NB100-384	152 Sm
Ki67	MKI67	Fluidigm	3168022D	168 Er
DNA				191 Ir

Figure Legends

Figure 1: Numbers of senescent glial cells are increased in brains of AD compared to those from NDC donors. *a) Multiplexed imaging mass cytometry (IMC) (scale bar = 50 µm) revealed overlapping expression of senescence (GLB1 and p16) and cell type specific markers (IBA1; microglia, OLIG2; oligodendrocyte lineage, GFAP; astrocyte) in cohort-1. b) Proportions of $GLB1^+$, $p16^+$ and $GLB1^+p16^+$ microglia ($IBA1^+$), oligodendrocyte ($OLIG2^+$) and astrocyte ($GFAP^+$) were calculated in AD and NDC using cohort-1 IMC data (Wilcoxon rank-sum test, *p <= 0.05. **p <= 0.01). c) UMAP showing the cellular clusters generated by SIMPLI from cohort-2 IMC data. d) Marker mean expression heatmap by clusters. e) Proportion of nuclei of all clusters expressing senescence markers in AD and NDC (Wilcoxon rank-sum test, p <= 0.1 is reported).*

Figure 2: The microglial transcriptome is enriched for senescence gene expression in AD. *a) Study design showing the three regions from each of the 17 brains from which nuclei were isolated to generate snRNAseq data. b) UMAP of seven distinct cell type populations characterized from snRNAseq data generated from 49 brain blocks. c) Dot plot showing average scaled expression of genes and percentage of cells expressed from the 'canonical senescence pathway (CSP)', the 'senescence initiating pathway (SIP)'* [16] *and a custom senescence set (Supplementary data S5) for each cell type. d) Normalised aggregated expression of genes as in (c) projected on UMAP. Color gradient scale showing aggregated gene set score in each nuclei. e) Box plot showing scaled mean expression of the CSP genes in each cell type (Wilcoxon rank-sum test). f) Percentage of senescent nuclei between AD and NDC across all cell types stratified by brain regions (Wilcoxon rank-sum test, *p <= 0.05) (Astro, astrocytes; Micro, microglia; Oligo, oligodendrocytes; OPC, Oligodendrocyte progenitor cells; Vasc, vascular cells; Exc, excitatory neurons, Inh; Inhibitory neurons).*

Figure 3: Senescence-associated genes are differentially expressed in microglia from AD and NDC donors. *a) Volcano plot showing differentially expressed genes between AD and NDC in microglia; senescence genes are annotated in blue. b,c) Barplots showing up- (b) and down-regulated (c) gene pathway enrichments in microglia with AD relative to NDC. d) Heatmap showing senescence and other relevant gene set enrichments in AD relative to NDC (adjusted p, *p<=0.05, **p<=0.01, ***p<=0.001).*

Figure 4: Senescence-associated genes are differentially expressed in microglia from AD and NDC donors. *A) IMC data (cohort-1) were used to quantify the number of cells positive for senescence markers GLB1, p16 or both by co-localizing them with the microglia specific marker IBA1 and 4G8^{+} β-amyloid plaque (yellow pixels). i and ii shows two plaque regions containing IBA1^{+} positive cells. IBA1^{+} microglia within 10 µm of plaques were defined as peri-plaque microglia. b) The proportion of peri-plaque microglia expressing senescence markers was significantly higher than for non-plaque microglia in AD (Wilcoxon rank-sum test, *p<=0.05, **p<=0.01, ***p<=0.001). c) Heatmap showing top 5 differentially expressed genes by logFC (adjusted p-value 0.05) against β-amyloid loads measured by 4G8^{+} immunohistochemical staining densities in all cell types in snRNAseq data. d) The gene expression graph illustrates its correlation with β-amyloid densities. The upper section displays the log2-normalized expression of each gene in individual nuclei, with median expression denoted by a black circle. The lower section indicates the percentage of non-zero nuclei in each sample.*

Figure 5: Sub-populations of microglia differentially express senescence gene signatures. *a) UMAP dimensionality reduction plot showing microglial sub-populations b) Odds-ratio estimates of microglial sub-populations associated with AD (circle; OR estimate obtained from MASC*[22]*, bars; 95% CI). c) Differences in relative numbers of each of the microglial sub-populations isolated from AD and NDC cortical brain tissue. d) Percentages of microglial sub-populations as a function of β-amyloid load (Micro2 Pearson's R = 0.63, p-value = 1.4e^{-06}). e) Boxplot showing normalised mean expression of the CSP gene set in the different microglial sub-populations (Wilcoxon rank-sum test). f) Bar plots comparing the proportions of senescent nuclei between AD and Control for Micro1-3 (Wilcoxon test, **p-value < 0.01). g) Correlations of the proportions of Micro1-3 senescent nuclei with β-amyloid (4G8^{+}) immunostained areas in sampled region of each brain (Micro1 Pearson's R = 0.34, p-value = 0.021). h) Boxplots showing the scaled mean expression of CSP gene set across microglial sub-population grouped by TREM2 genotype (CV, common allele, or the R47H AD risk variant).*

Figure 6: Sub-clustering of oligodendrocytes and astrocytes*. Sub-clustering of oligodendrocytes (a-b) and astrocytes (c-d) show diverse functional sub-populations. a, c) UMAP dimensionality reduction plots describing these sub-populations for oligodendroglia (a) and astrocytes (c). b, d) Normalised mean expression of CSP between AD and Control across sub-populations of oligodendrocytes (b) and astrocytes (d).*

Figure 7: Premature senescence of microglia with greater pseudo-time in AD is associated with gene signatures for inflammatory activation. *a) UMAP plot colored by microglial pseudo-time trajectory calculated by Monocle3* [71]*. b) Heatmap showing the relative enrichment of gene co-expression modules differentially expressed with increasing pseudo-time. Module names are colored according to pseudotime progression: Purple, early-; lilac, mid-; yellow, late-pseudotime c) Significantly enriched pathway of the co-expression module genes. Pathway names are colored according to plot (b). d) Network plot showing hub genes for each module (distinguished by colours) with senescence pathway associated genes highlighted (black circle).*

Supplementary figure 1: Representative IMC images showing overlapping expression of cell type and senescence markers. *Multiplexed imaging mass cytometry (IMC) (scale bar = 50 µm) revealed overlapping expression of a) microglia (IBA1), b) oligodendrocyte lineage (OLIG2) and c) astrocyte (GFAP) markers with senescence markers (GLB1 and p16). Orange*

arrowheads highlight senescent cells. d) Proportions of GLB1$^+$ endothelial cells (GLUT1$^+$) and neurons (MAP2$^+$) were calculated in AD and NDC using IMC.

Supplementary figure 2: Cells expressing senescence markers in entorhinal and somatosensory cortices detected by IMC*. a) Multiplexed imaging mass cytometry (IMC) revealed overlapping expression of DNA damage marker γH2AX and cell type specific markers (IBA1; microglia, MAP2; neuron, GFAP; astrocyte). Proportion of nuclei of all clusters expressing senescence markers in AD and NDC in b) entorhinal cortex (EC) and c) somatosensory cortex (SSC) (Wilcoxon rank-sum test, p <= 0.1 is reported).*

Supplementary figure 3: All cell clusters are equally represented in both AD and NDC groups*. a) UMAP showing the cellular clusters generated by SIMPLI from cohort-2 IMC data grouped by Control or AD in each brain regions. b) Proportions of all cell clusters identified by SIMPLI are equally represented in AD and Control.*

Supplementary figure 4: Canonical marker gene expression reveals distinct cell types. a) *UMAP featureplots of canonical cell marker genes for astrocytes (GFAP), microglia (CSFR1), oligodendrocytes (PLP1), oligodendrocyte precursor cells (PDGFRA), vascular cells (CLDN5, COL4A1, DCN) and neurons (GAD1, GAD2, CUX2, RORB, SST, PVALB, SV2C, VIP). b) Percentage of senescent nuclei between AD and NDC across all cell types (Wilcoxon rank-sum test, Astro, astrocytes; Micro, microglia; Oligo, oligodendrocytes; OPC, Oligodendrocyte progenitor cells; Vasc, vascular cells; Exc, excitatory neurons, Inh; Inhibitory neurons).*

Supplementary figure 5: Differential gene and pathway expression between AD and NDC cortical brain tissue for nuclei from different cell types. *Volcano plot showing differentially expressed genes in AD compared to NDC at logFC cut-off 0.25 and adjusted p-value cut-off 0.05 for a) astrocytes, b) oligodendrocytes, c) OPC, d) excitatory neurons and e) inhibitory neuron and f) vascular cells. Orange and blue bar plots are show major gene ontologies (GO Biological Processes) for upregulated or downregulated genes, respectively.*

Supplementary figure 6: Gene set enrichment analysis associated with increasing 4G8+ β-amyloid load. *a) Heatmap showing z-scores for enrichments in senescence gene sets associated with the same measures of β-amyloid pathology load across cell types. b, c) CSP gene set score per sample is plotted as a function of b) %4G$^+$ area (β-amyloid) densities and c) braak stages. Linear mixed model, adjusted pval is reported.*

Supplementary figure 7: Meta-analysis of senescence-associated gene expression in previously published AD snRNAseq datasets. *We re-analysed previously published datasets* [66]*) to explore senescence-associated gene expression upregulated in a) astrocytes or b) microglia with increasing %4G8$^+$ (β-amyloid) load. c) Forest plot showing the meta log2FC (orange diamond), meta p-value and log2FC effect sizes (red square) along with 95% CI (error bars) of "canonical senescence pathway" gene set expression between AD and NDC samples in individual datasets calculated from the meta-analysis of 14 previously published AD snRNAseq datasets. d) Contrast of the mean CSP gene set scores as a function of age for AD and NDC samples. Linear plateau modelling, pval is reported.*

Supplementary figure 8: Gene Ontology (GO) pathway enrichment in genes up- and down-regulated with greater 4G8^{+} β-amyloid areas in tissue sections paired to those for snRNAseq. *Top significantly enriched pathways from regression of gene expression against %4G8^{+}(β-amyloid) area for a) upregulated and b) downregulated genes from each cell type. Pathways were considered significant at 0.05 FDR.*

Supplementary figure 9: Senescence-associated gene signatures were differentially expressed for different microglia sub-types. *a) Heatmap showing the top 5 marker genes distinguishing microglial sub-types. b) Mean expression of marker gene sets* [47] *distinguishing microglial sub-populations. c) Enrichment of marker gene sets from* [23] *in the markers detected in microglial sub-populations in this study. d, e) UMAP color-scaled featureplots showing total numbers of genes expressed (d) and the percentages of mitochondrial genes (e) in microglia nuclei highlighting that increased relative proportions of senescence genes are expressed in nuclei expressing lower mitochondrial gene numbers. f, g) Percentages of senescent nuclei in AD and NDC (f) and as a function of 4G8^{+} β-amyloid load (g) for the major microglial sub-types stratified by brain region. h, i) Boxplots showing the scaled mean expression of canonical senescence gene set across microglial sub-population grouped by h) CD33 variants and i) APOE variants.*

Supplementary figure 10: Oligodendrocyte and astrocyte subcluster characterisation*. a) Heatmap showing the top 5 marker genes distinguishing oligodendrocytes subpopulations. b) Dotplot showing enrichment of external marker genes* [33, 48] *for oligodendrocyte sub-clusters across the sub-population identified in this study. c) Heatmap showing the top 5 marker genes distinguishing astrocyte subpopulations.*

Supplementary figure 11: Microglial sub-population changes as a function of age*. a, b) Percentages of nuclei for microglial sub-populations as a function of donor age at death in this study cohort-2 (a) and in the integrated data used for the meta-analysis (b).*

Supplementary figure 12: Microglia trajectory module featureplots*. a) Module featureplots showing the expression of gene modules derived from microglial trajectory analyses. b) Module-5 gene set expression as a function of %4G8^{+} densities.*

Fig 1

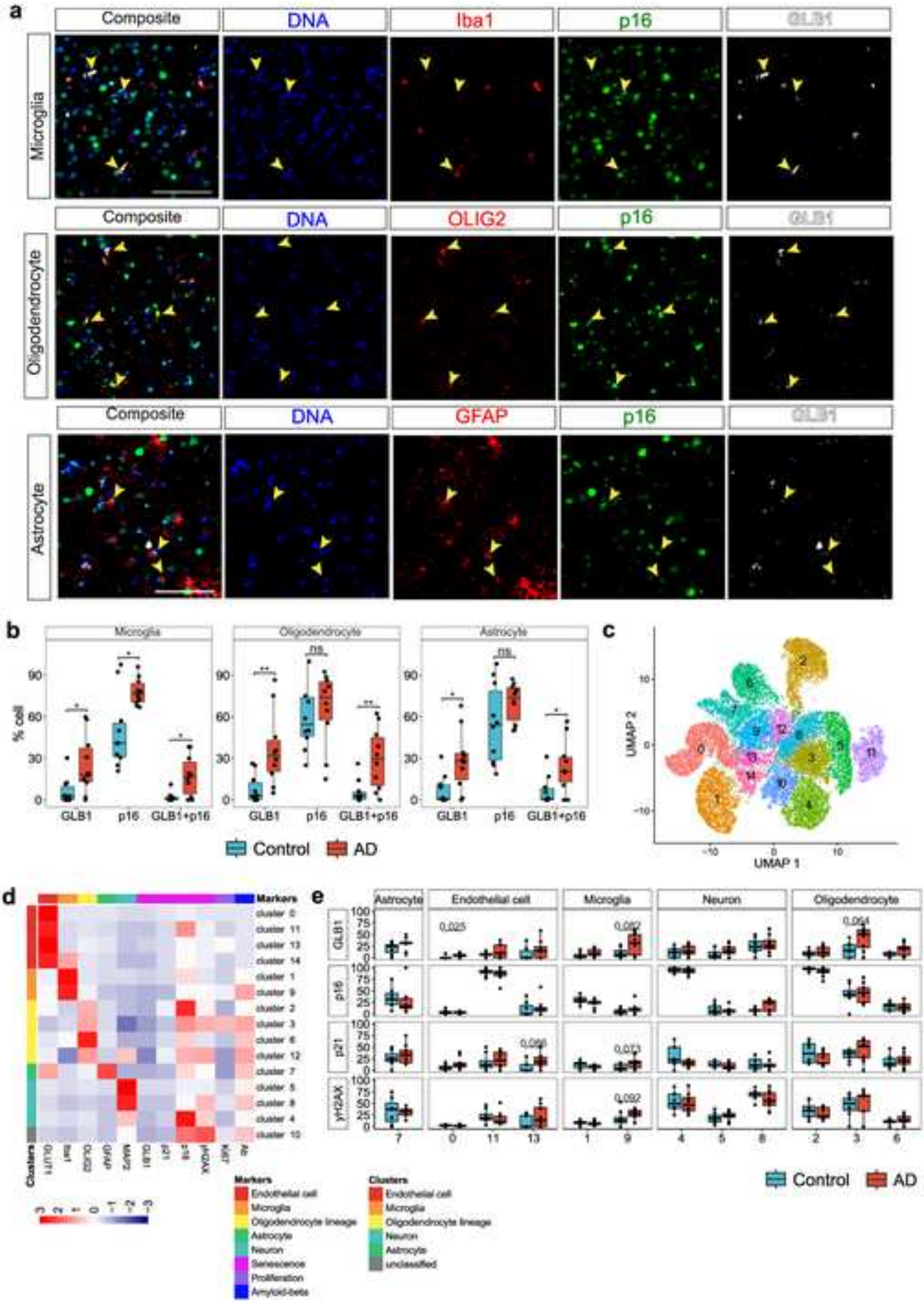
a
Composite
DNA
Iba1
p16
GLB1
Microglia
Composite
DNA
OLIG2
p16
GLB1
Oligodendrocyte
Composite
DNA
GFAP
p16
GLB1
Astrocyte
b
Microglia
Oligodendrocyte
Astrocyte
% cell
GLB1
p16
GLB1+p16
Control
AD
c
UMAP 1
UMAP 2
d
Markers
Clusters
e
Astrocyte
Endothelial cell
Microglia
Neuron
Oligodendrocyte
GLB1
p16
p21
γH2AX
Control
AD

Fig 2

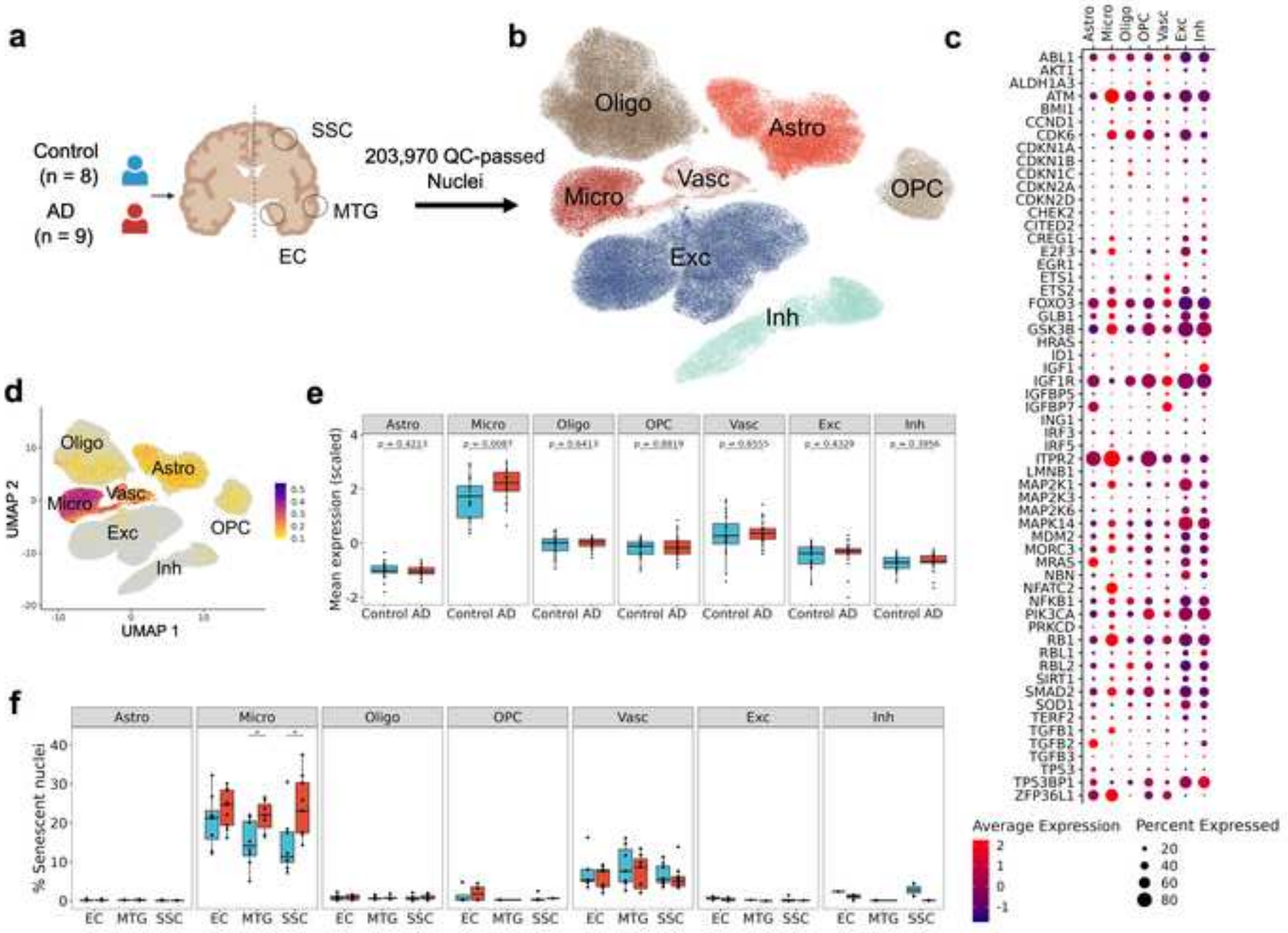
a
Control
(n = 8)
AD
(n = 9)
SSC
MTG
EC
203,970 QC-passed
Nuclei
b
Oligo
Astro
Vasc
Micro
OPC
Exc
Inh
c
Astro
Micro
Oligo
OPC
Vasc
Exc
Inh
ABL1
AKT1
ALDH1A3
ATM
BMI1
CCND1
CDK6
CDKN1A
CDKN1B
CDKN1C
CDKN2A
CDKN2D
CHEK2
CITED2
CREG1
E2F3
EGR1
ETS1
ETS2
FOXO3
GLB1
GSK3B
HRAS
ID1
IGF1
IGF1R
IGFBP5
IGFBP7
ING1
IRF3
IRF5
ITPR2
LMNB1
MAP2K1
MAP2K3
MAP2K6
MAPK14
MDM2
MORC3
MRAS
NBN
NFATC2
NFKB1
PIK3CA
PRKCD
RB1
RBL1
RBL2
SIRT1
SMAD2
SOD1
TERF2
TGFB1
TGFB2
TGFB3
TP53
TP53BP1
ZFP36L1
Average Expression
Percent Expressed
d
UMAP 2
UMAP 1
e
Mean expression (scaled)
Control AD
f
% Senescent nuclei
EC MTG SSC

Fig 3

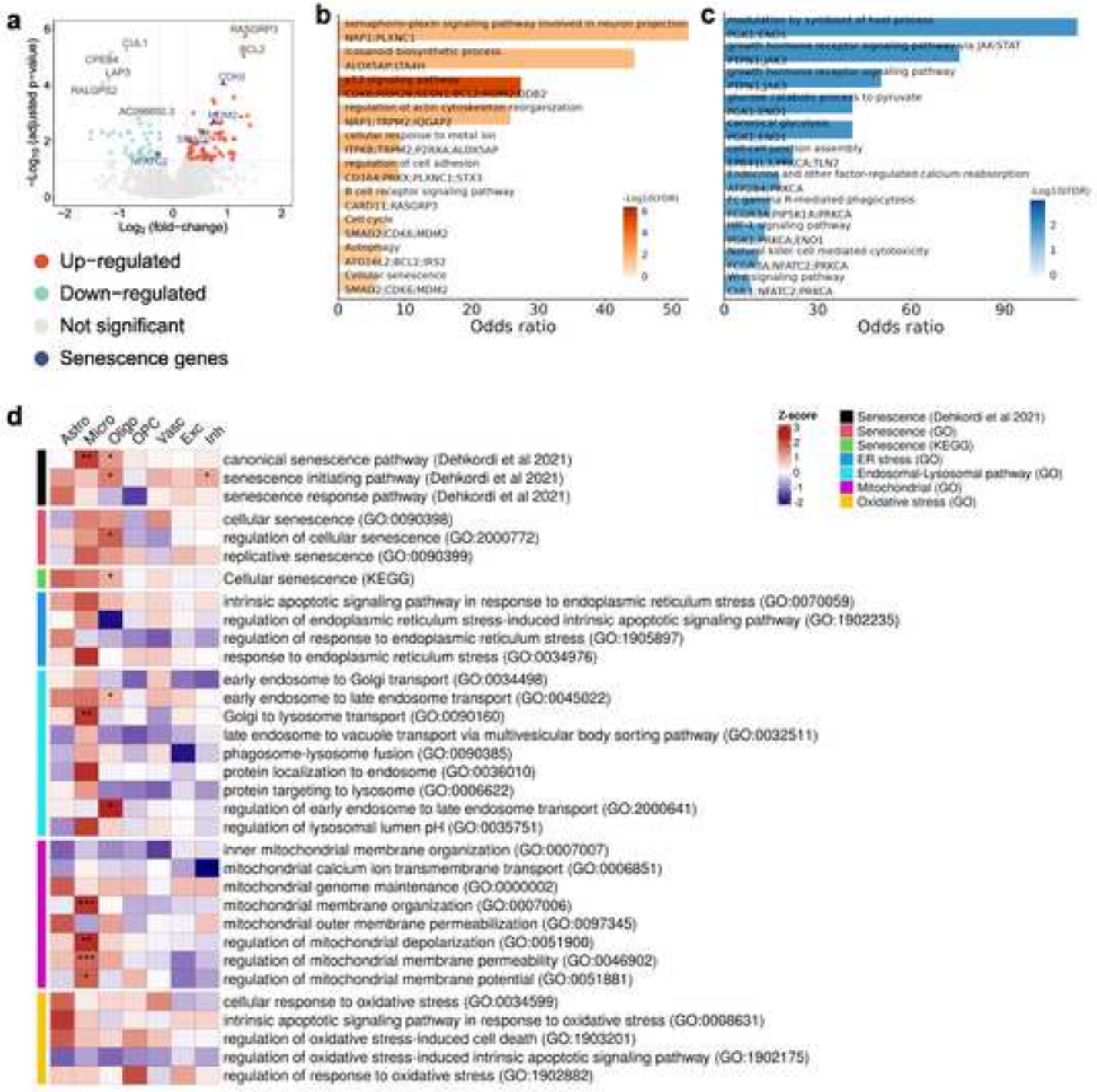
a
Up−regulated
Down−regulated
Not significant
Senescence genes
Log2 (fold−change)
−Log10 (adjusted p−value)
b
Odds ratio
c
Odds ratio
d
Astro
Micro
Oligo
OPC
Vasc
Exc
Inh
Z-score
Senescence (Dehkordi et al 2021)
Senescence (GO)
Senescence (KEGG)
ER stress (GO)
Endosomal-Lysosomal pathway (GO)
Mitochondrial (GO)
Oxidative stress (GO)
canonical senescence pathway (Dehkordi et al 2021)
senescence initiating pathway (Dehkordi et al 2021)
senescence response pathway (Dehkordi et al 2021)
cellular senescence (GO:0090398)
regulation of cellular senescence (GO:2000772)
replicative senescence (GO:0090399)
Cellular senescence (KEGG)
intrinsic apoptotic signaling pathway in response to endoplasmic reticulum stress (GO:0070059)
regulation of endoplasmic reticulum stress-induced intrinsic apoptotic signaling pathway (GO:1902235)
regulation of response to endoplasmic reticulum stress (GO:1905897)
response to endoplasmic reticulum stress (GO:0034976)
early endosome to Golgi transport (GO:0034498)
early endosome to late endosome transport (GO:0045022)
Golgi to lysosome transport (GO:0090160)
late endosome to vacuole transport via multivesicular body sorting pathway (GO:0032511)
phagosome-lysosome fusion (GO:0090385)
protein localization to endosome (GO:0036010)
protein targeting to lysosome (GO:0006622)
regulation of early endosome to late endosome transport (GO:2000641)
regulation of lysosomal lumen pH (GO:0035751)
inner mitochondrial membrane organization (GO:0007007)
mitochondrial calcium ion transmembrane transport (GO:0006851)
mitochondrial genome maintenance (GO:0000002)
mitochondrial membrane organization (GO:0007006)
mitochondrial outer membrane permeabilization (GO:0097345)
regulation of mitochondrial depolarization (GO:0051900)
regulation of mitochondrial membrane permeability (GO:0046902)
regulation of mitochondrial membrane potential (GO:0051881)
cellular response to oxidative stress (GO:0034599)
intrinsic apoptotic signaling pathway in response to oxidative stress (GO:0008631)
regulation of oxidative stress-induced cell death (GO:1903201)
regulation of oxidative stress-induced intrinsic apoptotic signaling pathway (GO:1902175)
regulation of response to oxidative stress (GO:1902882)

Fig 4

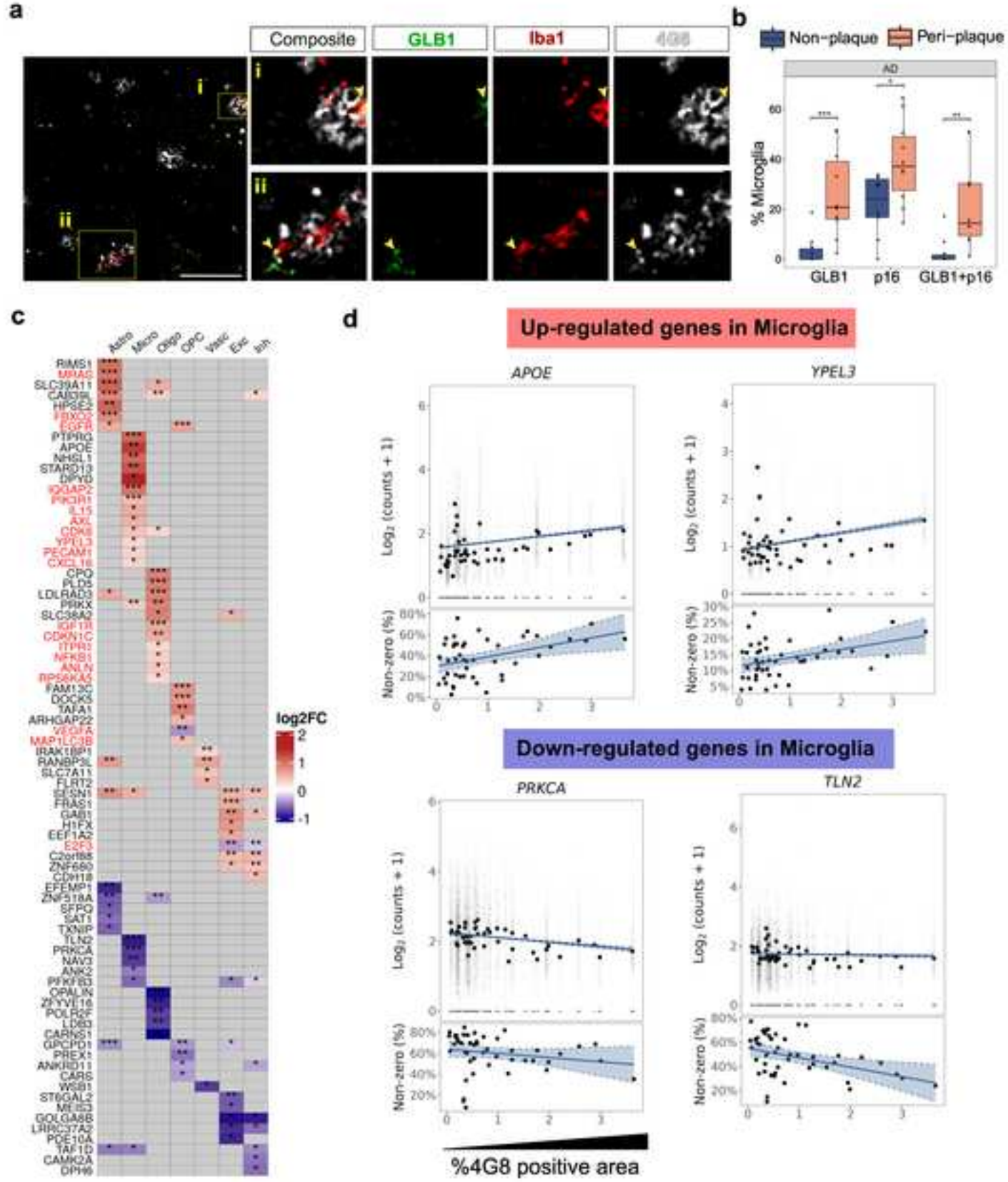
a
Composite
GLB1
Iba1
4G8
i
ii
b
Non-plaque
Peri-plaque
AD
% Microglia
GLB1
p16
GLB1+p16
c
Astro
Micro
Oligo
OPC
Vasc
Exc
Inh
log2FC
d
Up-regulated genes in Microglia
APOE
YPEL3
Down-regulated genes in Microglia
PRKCA
TLN2
Log2 (counts + 1)
Non-zero (%)
%4G8 positive area

Fig 5

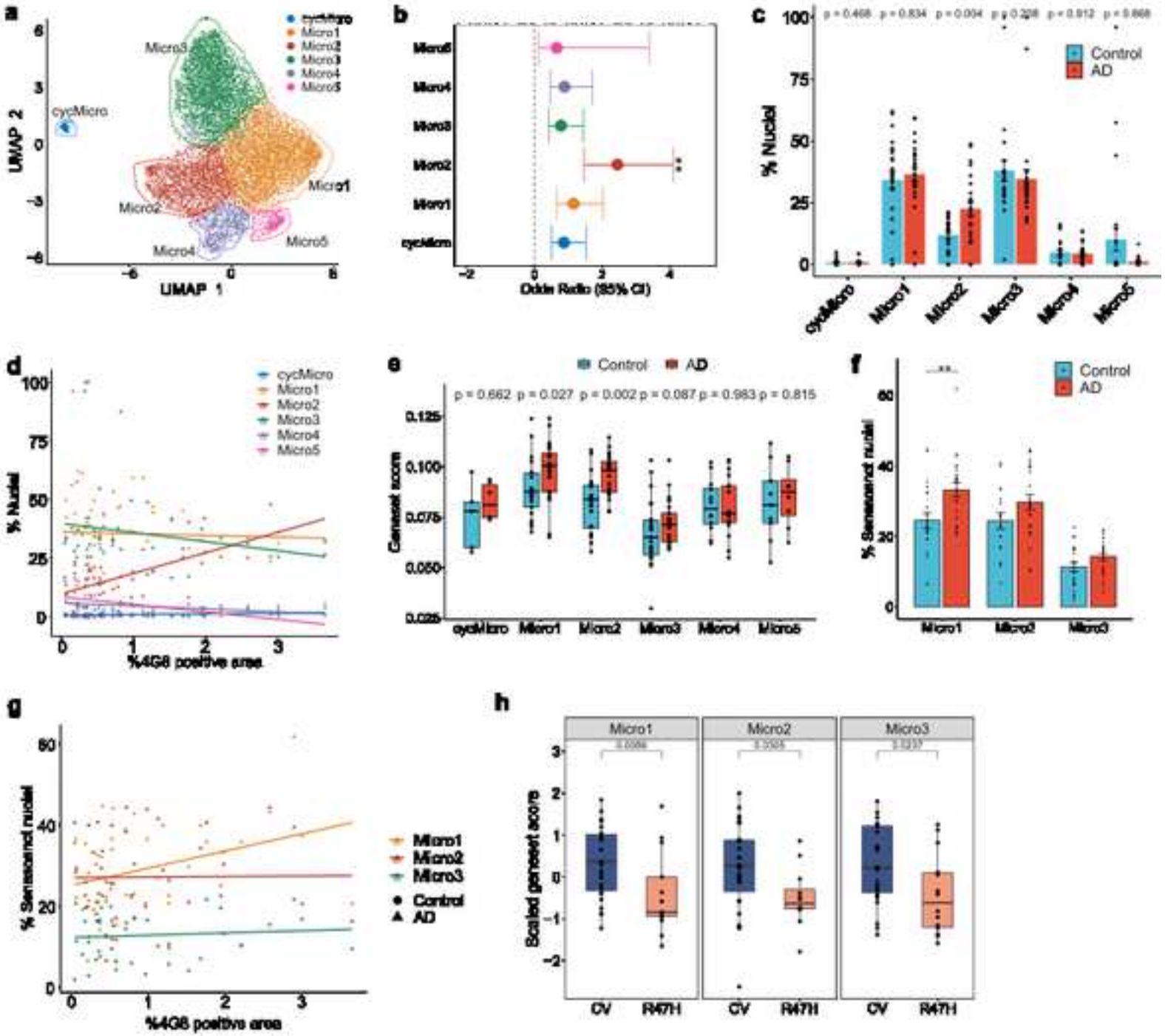
a
UMAP 2
UMAP 1
cycMicro
Micro1
Micro2
Micro3
Micro4
Micro5
b
Odds Ratio (95% CI)
c
% Nuclei
Control
AD
d
% Nuclei
%4G8 positive area
e
Control
AD
Geneset score
f
Control
AD
% Senescent nuclei
g
% Senescent nuclei
%4G8 positive area
Micro1
Micro2
Micro3
Control
AD
h
Micro1
Micro2
Micro3
Scaled geneset score
CV
R47H

Fig 6

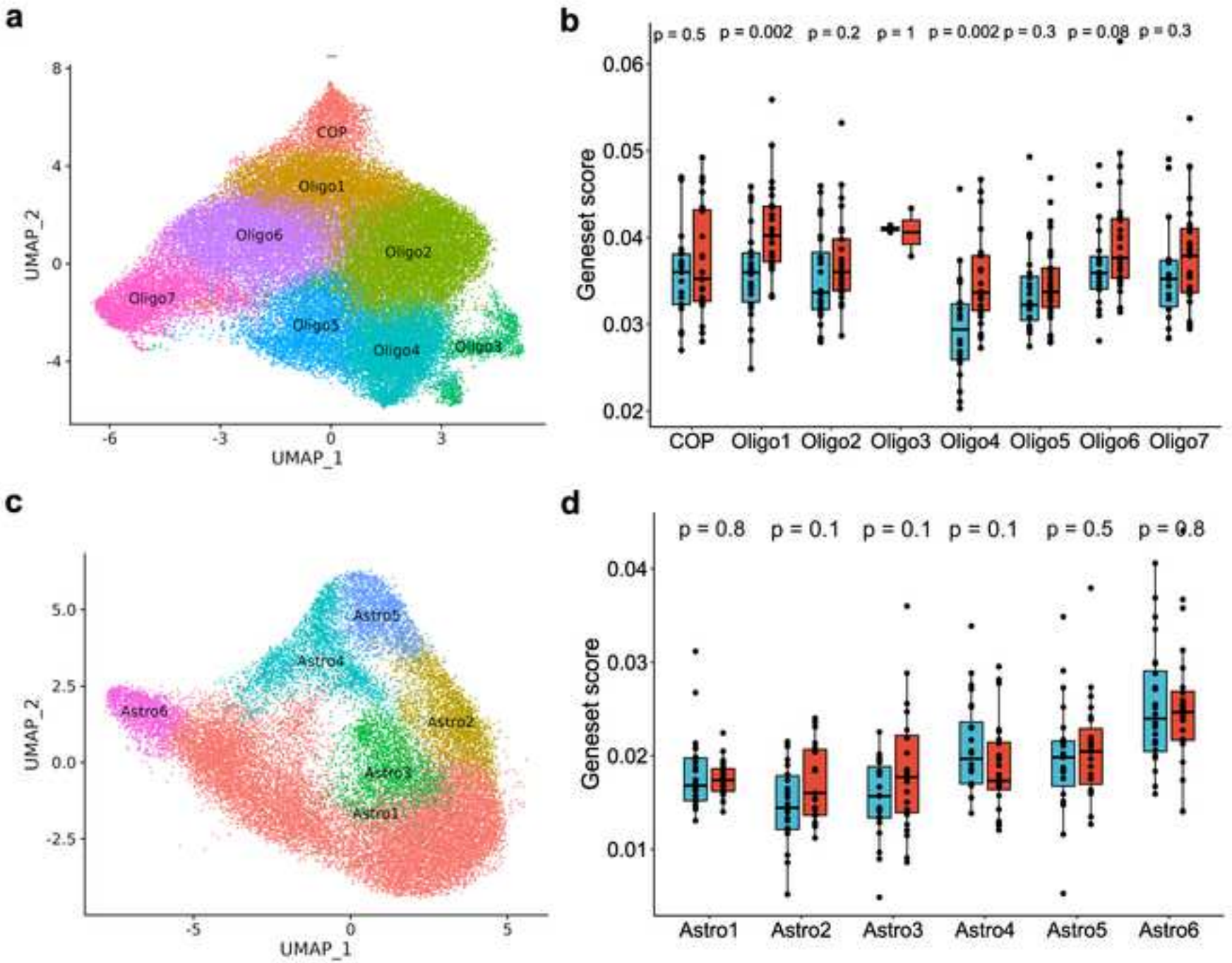
a
COP
Oligo1
Oligo6
Oligo2
Oligo7
Oligo5
Oligo4
Oligo3
UMAP_2
UMAP_1
b
p = 0.5 p = 0.002 p = 0.2 p = 1 p = 0.002 p = 0.3 p = 0.08 p = 0.3
Geneset score
COP Oligo1 Oligo2 Oligo3 Oligo4 Oligo5 Oligo6 Oligo7
c
Astro5
Astro4
Astro6
Astro2
Astro3
Astro1
UMAP_2
UMAP_1
d
p = 0.8 p = 0.1 p = 0.1 p = 0.1 p = 0.5 p = 0.8
Geneset score
Astro1 Astro2 Astro3 Astro4 Astro5 Astro6

Fig 7

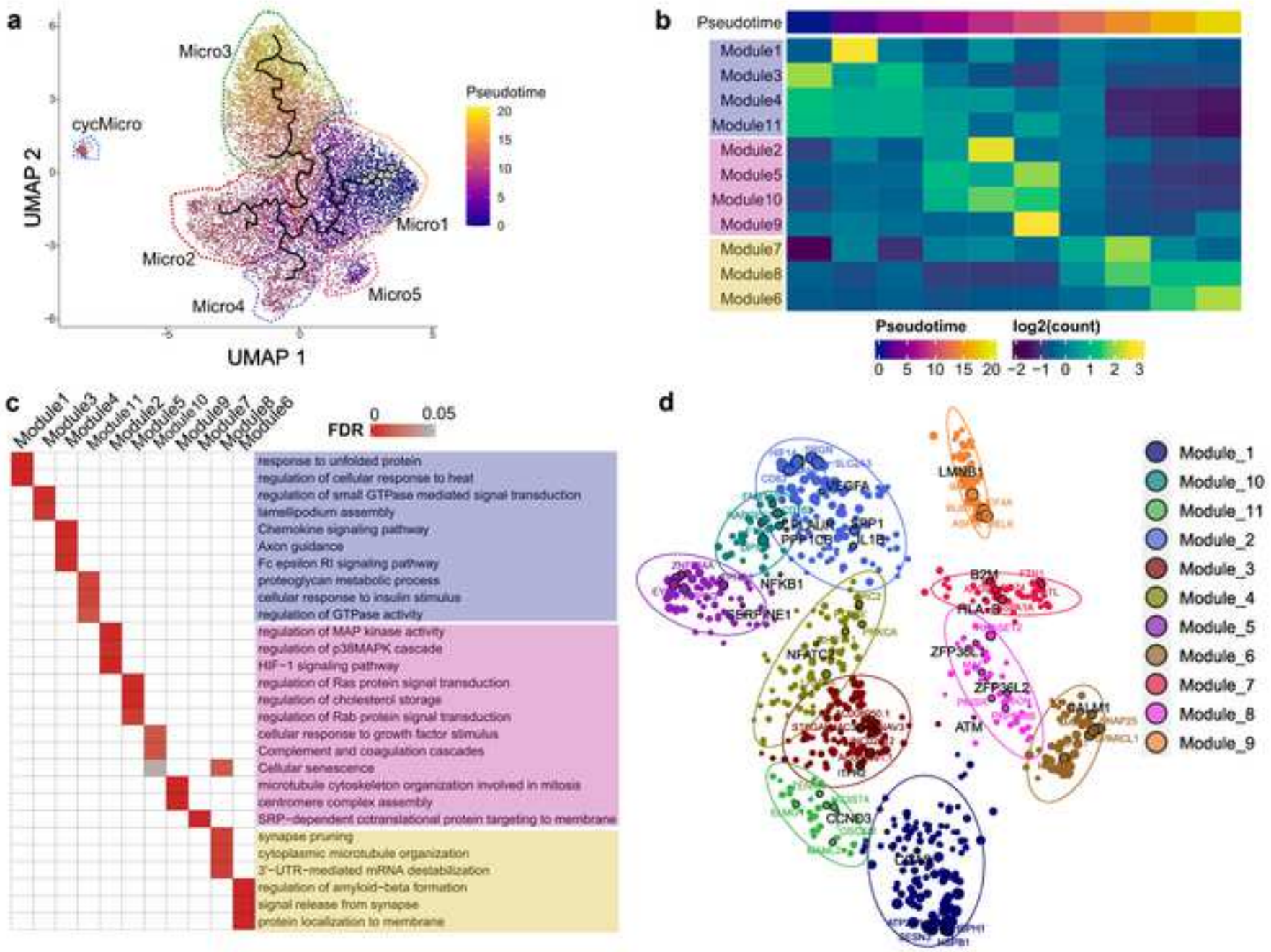
a
Micro3
cycMicro
Micro1
Micro2
Micro4
Micro5
UMAP 2
UMAP 1
Pseudotime
20
15
10
5
0
b
Pseudotime
Module1
Module3
Module4
Module11
Module2
Module5
Module10
Module9
Module7
Module8
Module6
Pseudotime
0 5 10 15 20
log2(count)
−2 −1 0 1 2 3
c
Module1
Module3
Module4
Module11
Module2
Module5
Module10
Module9
Module7
Module8
Module6
FDR
0
0.05
response to unfolded protein
regulation of cellular response to heat
regulation of small GTPase mediated signal transduction
lamellipodium assembly
Chemokine signaling pathway
Axon guidance
Fc epsilon RI signaling pathway
proteoglycan metabolic process
cellular response to insulin stimulus
regulation of GTPase activity
regulation of MAP kinase activity
regulation of p38MAPK cascade
HIF−1 signaling pathway
regulation of Ras protein signal transduction
regulation of cholesterol storage
regulation of Rab protein signal transduction
cellular response to growth factor stimulus
Complement and coagulation cascades
Cellular senescence
microtubule cytoskeleton organization involved in mitosis
centromere complex assembly
SRP−dependent cotranslational protein targeting to membrane
synapse pruning
cytoplasmic microtubule organization
3'−UTR−mediated mRNA destabilization
regulation of amyloid−beta formation
signal release from synapse
protein localization to membrane
d
VEGFA
SRP1
PPP1CB
IL1B
NFKB1
SERPINE1
NFATC2
ITPR2
CCND3
LMNB1
B2M
HLA-B
ZFP36L1
ZFP36L2
ATM
Module_1
Module_10
Module_11
Module_2
Module_3
Module_4
Module_5
Module_6
Module_7
Module_8
Module_9

Fig S1

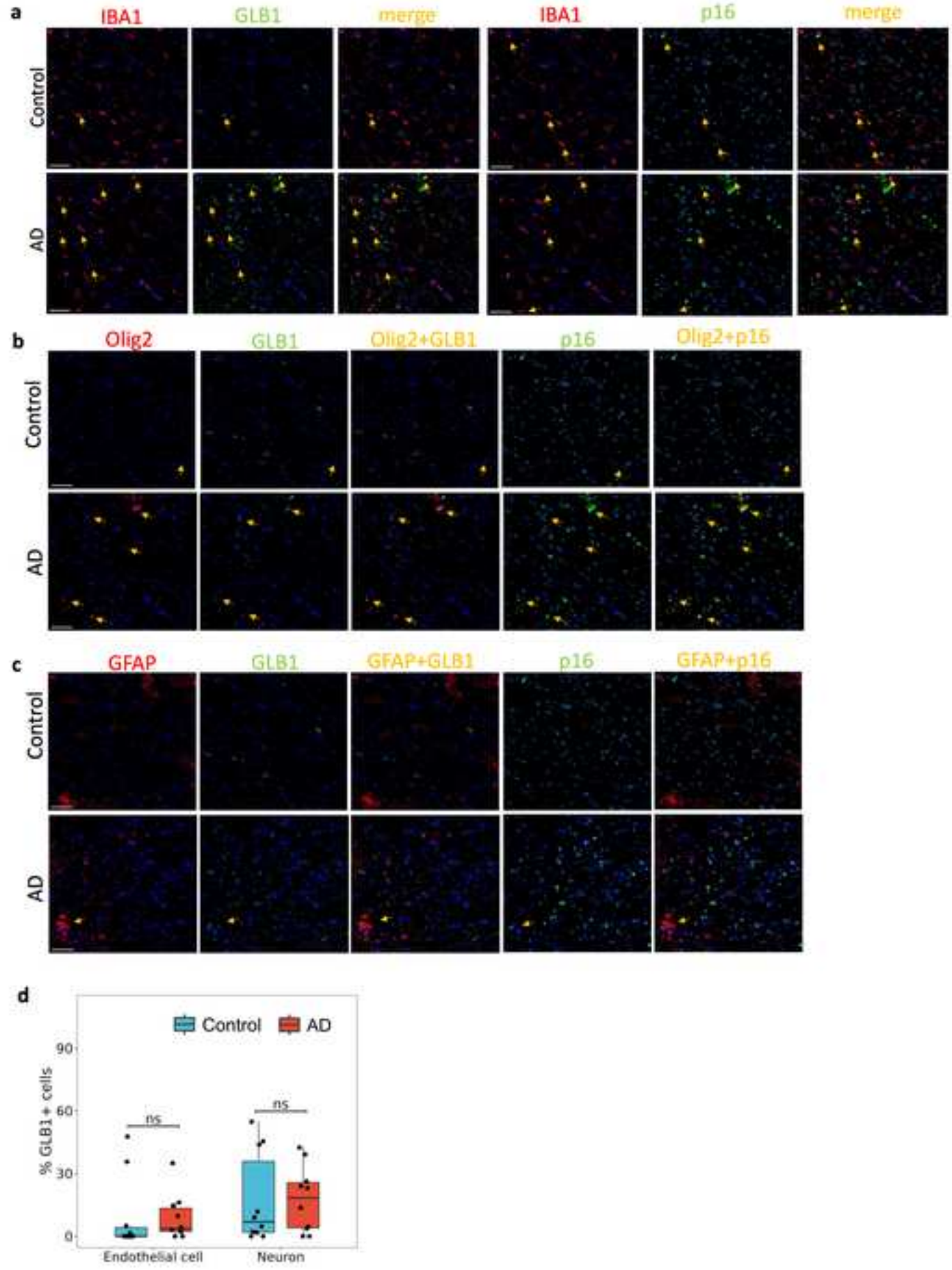
a
IBA1
GLB1
merge
IBA1
p16
merge
Control
AD
b
Olig2
GLB1
Olig2+GLB1
p16
Olig2+p16
Control
AD
c
GFAP
GLB1
GFAP+GLB1
p16
GFAP+p16
Control
AD
d
Control
AD
% GLB1+ cells
90
60
30
0
ns
ns
Endothelial cell
Neuron

Fig S2

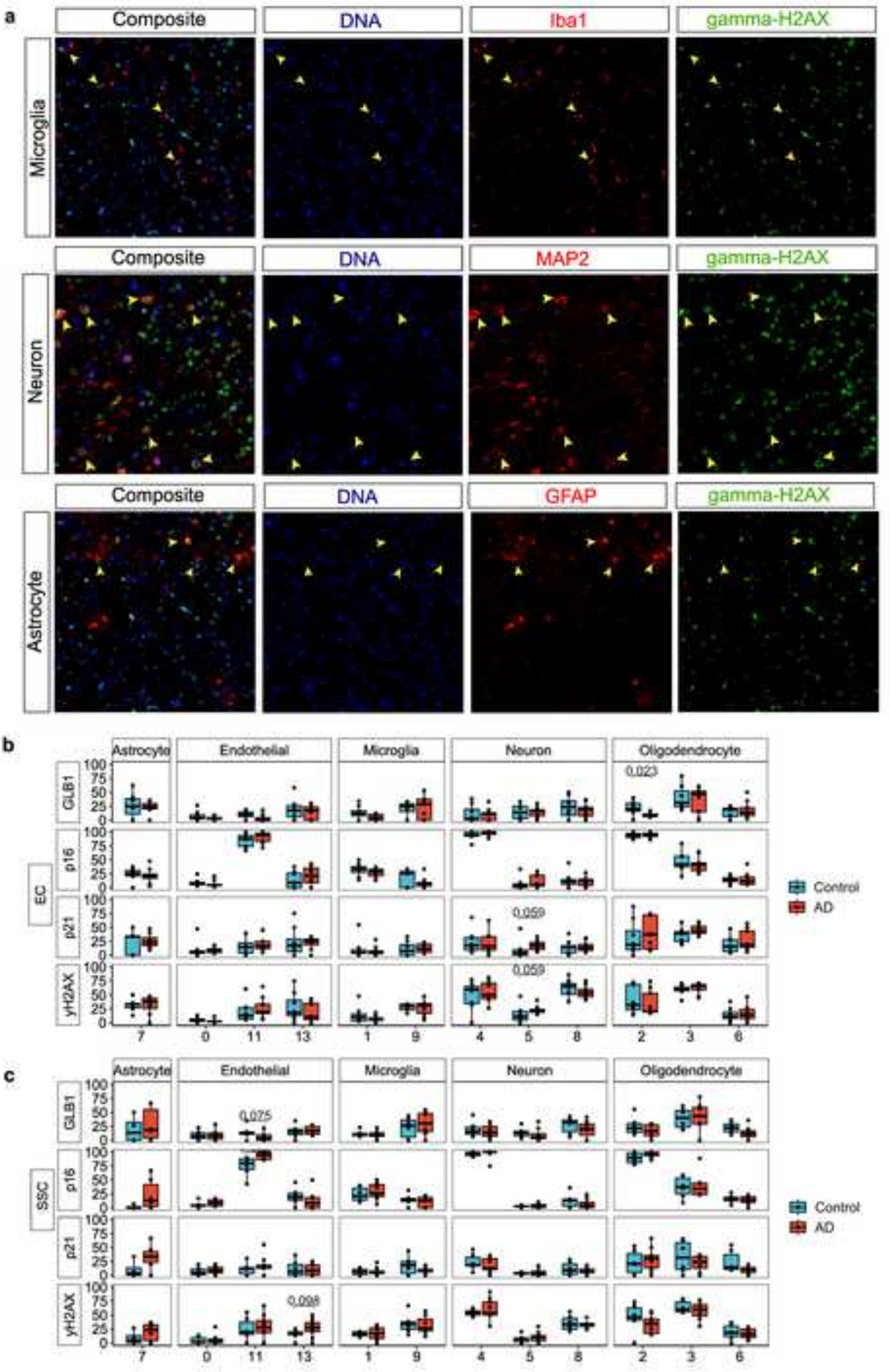
a
Composite
DNA
Iba1
gamma-H2AX
Microglia
Composite
DNA
MAP2
gamma-H2AX
Neuron
Composite
DNA
GFAP
gamma-H2AX
Astrocyte
b
Astrocyte
Endothelial
Microglia
Neuron
Oligodendrocyte
GLB1
p16
p21
γH2AX
EC
0.023
0.059
0.059
7
0
11
13
1
9
4
5
8
2
3
6
Control
AD
c
Astrocyte
Endothelial
Microglia
Neuron
Oligodendrocyte
GLB1
p16
p21
γH2AX
SSC
0.075
0.098
7
0
11
13
1
9
4
5
8
2
3
6
Control
AD

Fig S3

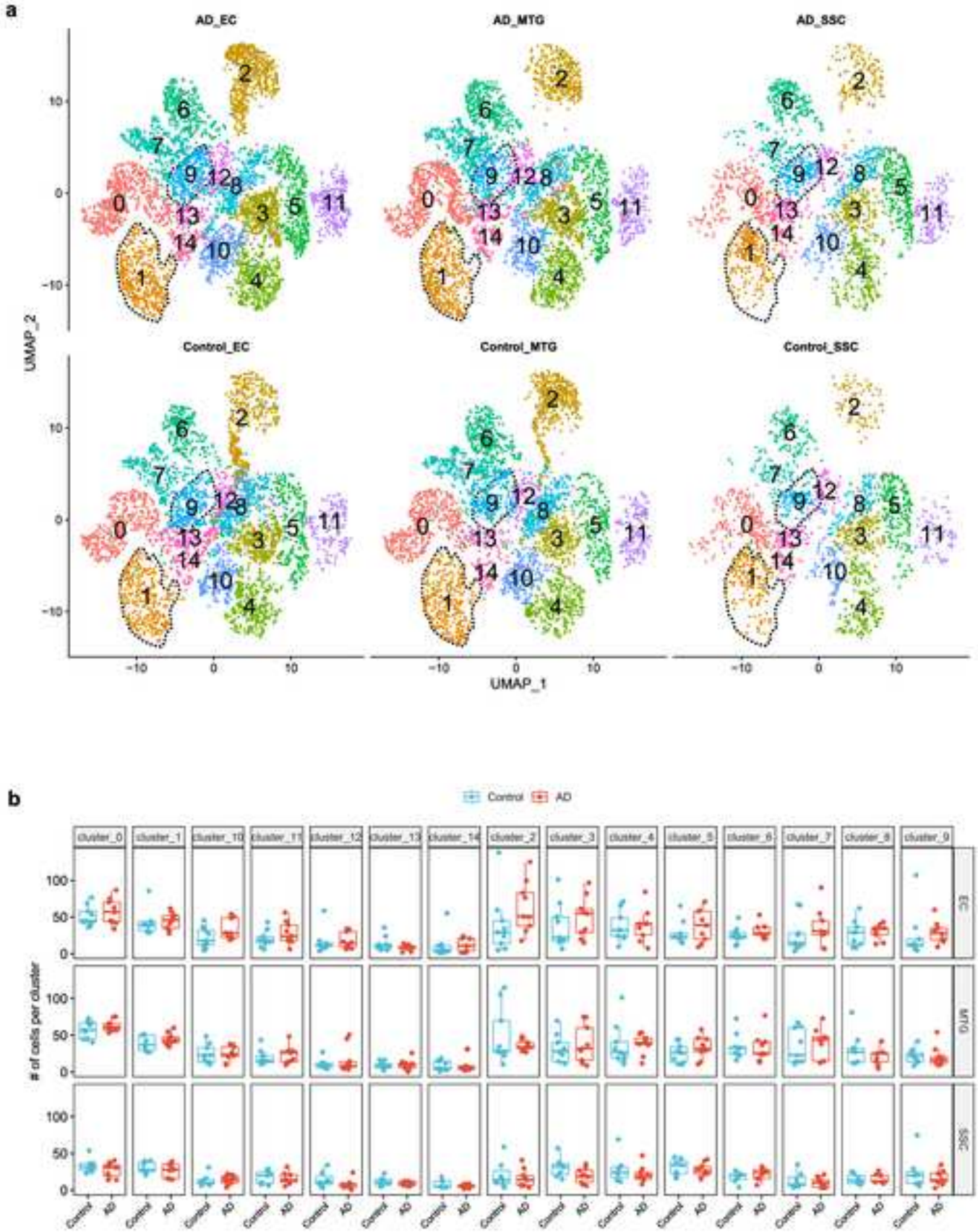
a
AD_EC
AD_MTG
AD_SSC
Control_EC
Control_MTG
Control_SSC
UMAP_2
UMAP_1
b
Control
AD
# of cells per cluster
EC
MTG
SSC

Fig S4

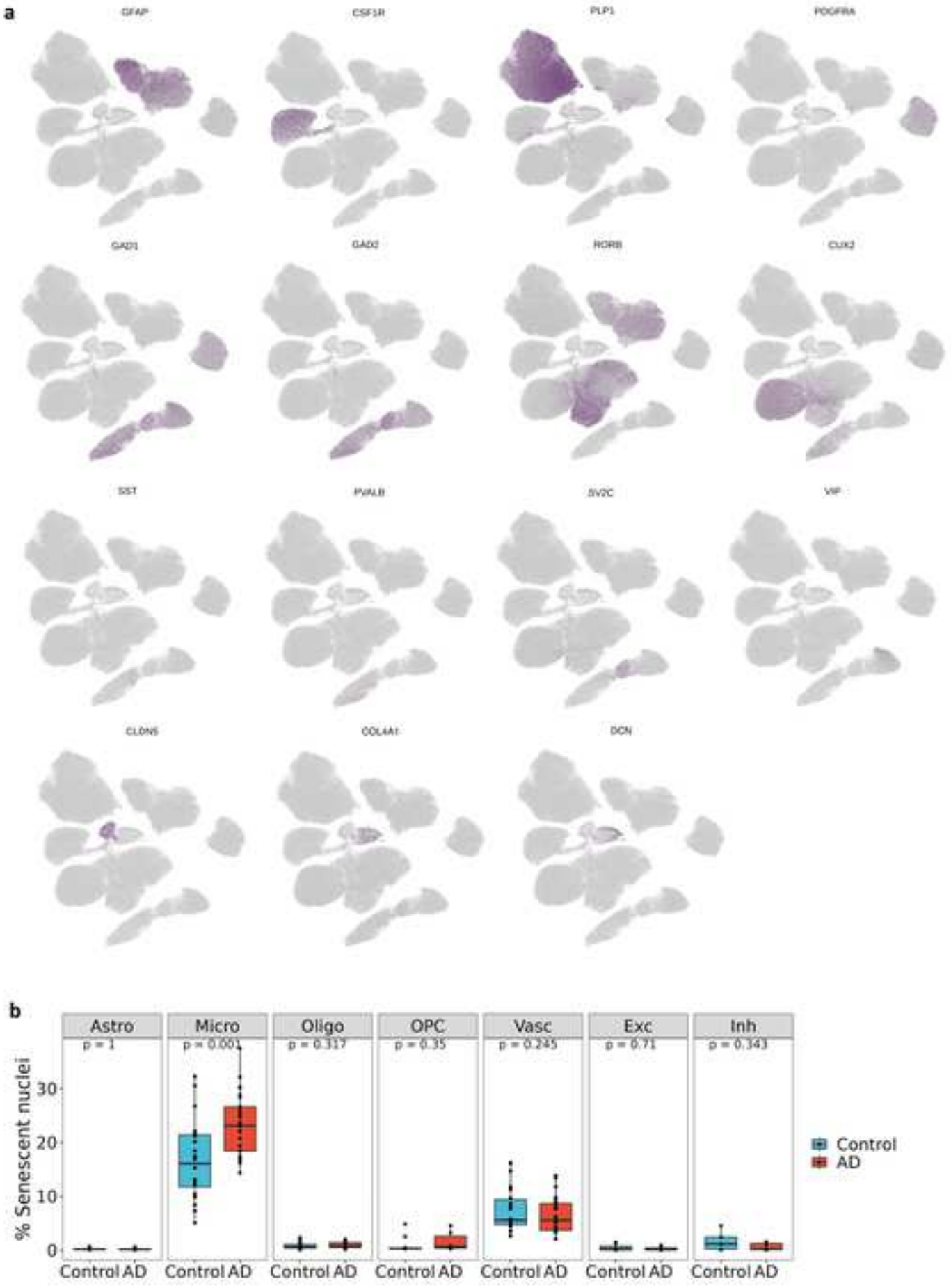
a
GFAP
CSF1R
PLP1
PDGFRA
GAD1
GAD2
RORB
CUX2
SST
PVALB
SV2C
VIP
CLDN5
COL4A1
DCN
b
Astro
Micro
Oligo
OPC
Vasc
Exc
Inh
p = 1
p = 0.001
p = 0.317
p = 0.35
p = 0.245
p = 0.71
p = 0.343
% Senescent nuclei
0
10
20
30
Control AD
Control
AD

Fig S5

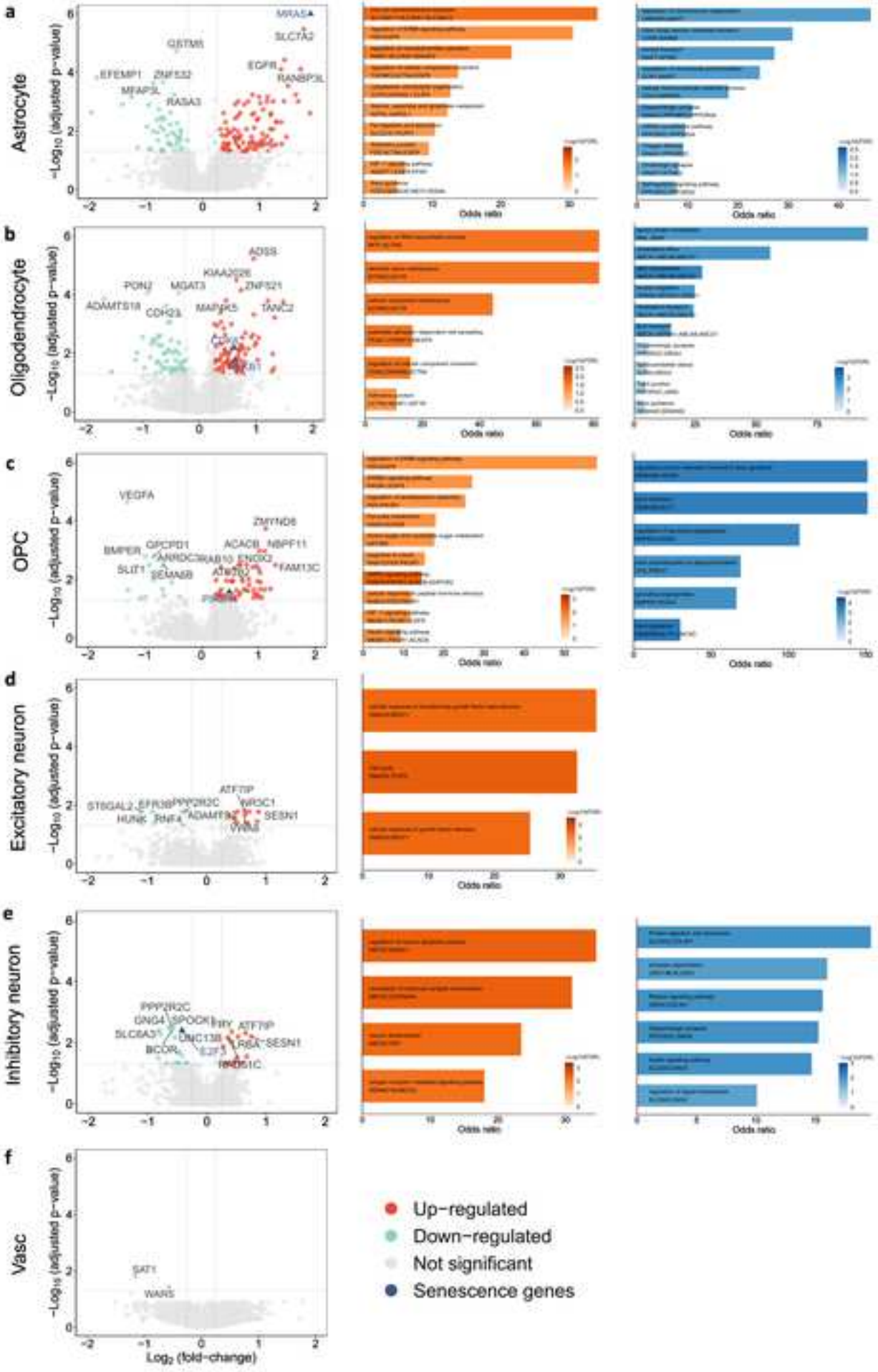
a
Astrocyte
b
Oligodendrocyte
c
OPC
d
Excitatory neuron
e
Inhibitory neuron
f
Vasc
−Log10 (adjusted p−value)
Log2 (fold−change)
Odds ratio
Up−regulated
Down−regulated
Not significant
Senescence genes

Fig S6

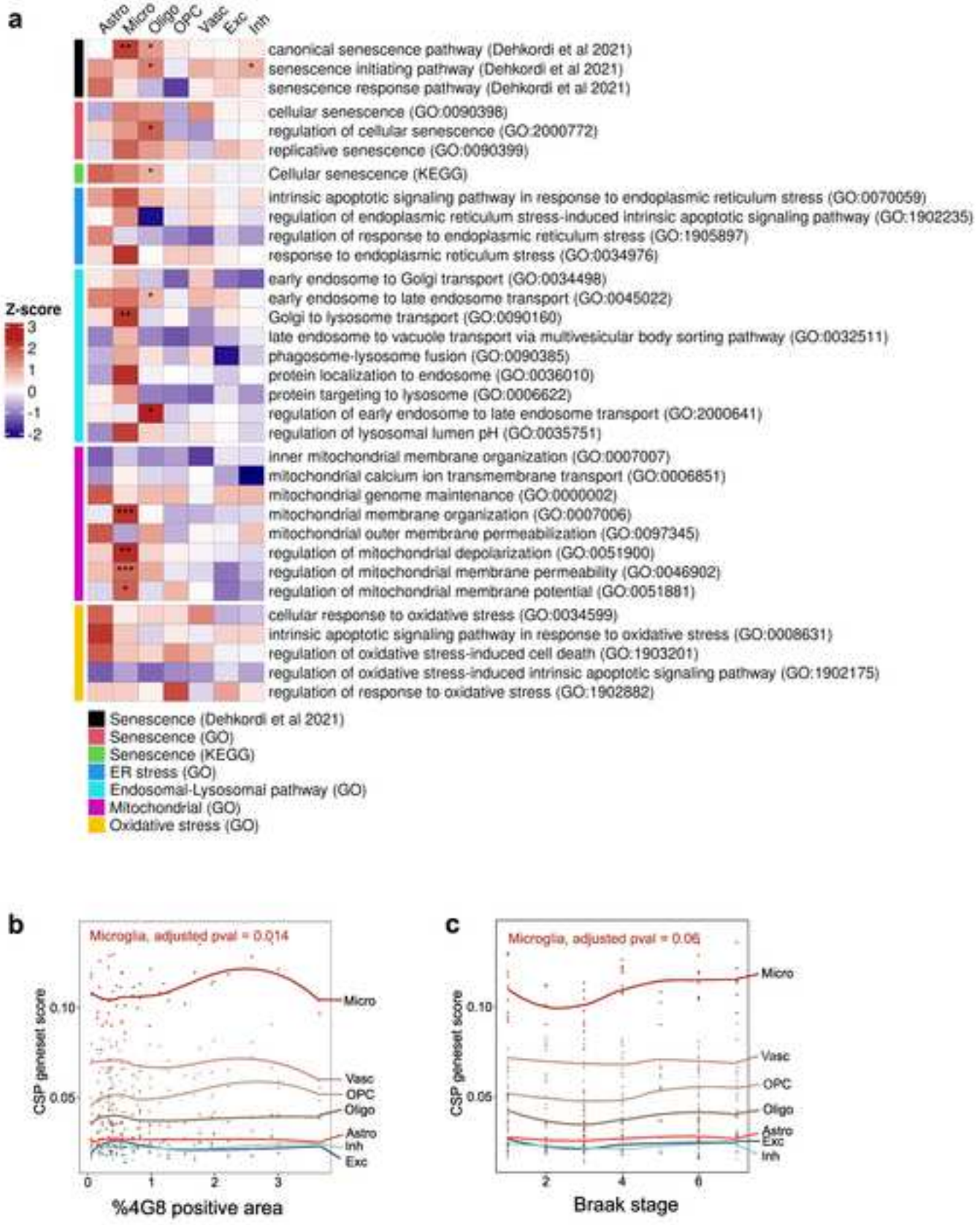
a
Astro
Micro
Oligo
OPC
Vasc
Exc
Inh
canonical senescence pathway (Dehkordi et al 2021)
senescence initiating pathway (Dehkordi et al 2021)
senescence response pathway (Dehkordi et al 2021)
cellular senescence (GO:0090398)
regulation of cellular senescence (GO:2000772)
replicative senescence (GO:0090399)
Cellular senescence (KEGG)
intrinsic apoptotic signaling pathway in response to endoplasmic reticulum stress (GO:0070059)
regulation of endoplasmic reticulum stress-induced intrinsic apoptotic signaling pathway (GO:1902235)
regulation of response to endoplasmic reticulum stress (GO:1905897)
response to endoplasmic reticulum stress (GO:0034976)
early endosome to Golgi transport (GO:0034498)
early endosome to late endosome transport (GO:0045022)
Golgi to lysosome transport (GO:0090160)
late endosome to vacuole transport via multivesicular body sorting pathway (GO:0032511)
phagosome-lysosome fusion (GO:0090385)
protein localization to endosome (GO:0036010)
protein targeting to lysosome (GO:0006622)
regulation of early endosome to late endosome transport (GO:2000641)
regulation of lysosomal lumen pH (GO:0035751)
inner mitochondrial membrane organization (GO:0007007)
mitochondrial calcium ion transmembrane transport (GO:0006851)
mitochondrial genome maintenance (GO:0000002)
mitochondrial membrane organization (GO:0007006)
mitochondrial outer membrane permeabilization (GO:0097345)
regulation of mitochondrial depolarization (GO:0051900)
regulation of mitochondrial membrane permeability (GO:0046902)
regulation of mitochondrial membrane potential (GO:0051881)
cellular response to oxidative stress (GO:0034599)
intrinsic apoptotic signaling pathway in response to oxidative stress (GO:0008631)
regulation of oxidative stress-induced cell death (GO:1903201)
regulation of oxidative stress-induced intrinsic apoptotic signaling pathway (GO:1902175)
regulation of response to oxidative stress (GO:1902882)
Z-score
3
2
1
0
-1
-2
Senescence (Dehkordi et al 2021)
Senescence (GO)
Senescence (KEGG)
ER stress (GO)
Endosomal-Lysosomal pathway (GO)
Mitochondrial (GO)
Oxidative stress (GO)
b
Microglia, adjusted pval = 0.014
CSP geneset score
0.10
0.05
Micro
Vasc
OPC
Oligo
Astro
Inh
Exc
0
1
2
3
%4G8 positive area
c
Microglia, adjusted pval = 0.06
CSP geneset score
0.10
0.05
Micro
Vasc
OPC
Oligo
Astro
Exc
Inh
2
4
6
Braak stage

Fig S7

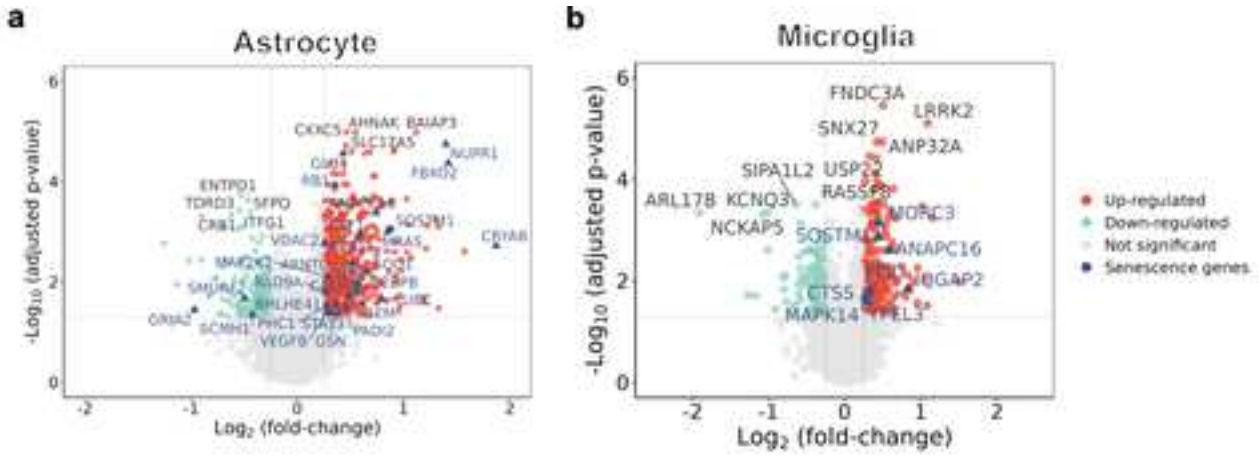

c

Study	Brain Region	Control (n)	AD (n)
ROSMAP	DLPFC	48	48
Grubman et al 2019	EC	5	6
Leng et al 2021	EC	6	3
This study	EC	8	9
SEA AD	MTG	41	40
This study	MTG	8	7
Gerrits et al 2021	OC	8	10
Gerrits et al 2021	OTC	8	10
Lao et al 2020	PFC	9	11
Mathys et al 2019	PFC	9	32
Morabito et al 2021	PFC	7	11
Zhou et al 2020	PFC	11	11
Leng et al 2021	SFG	7	3
This study	SSC	8	9
Summary		**183**	**210**

meta p = 7e-04

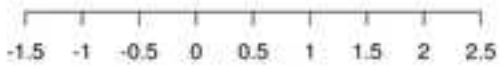

d

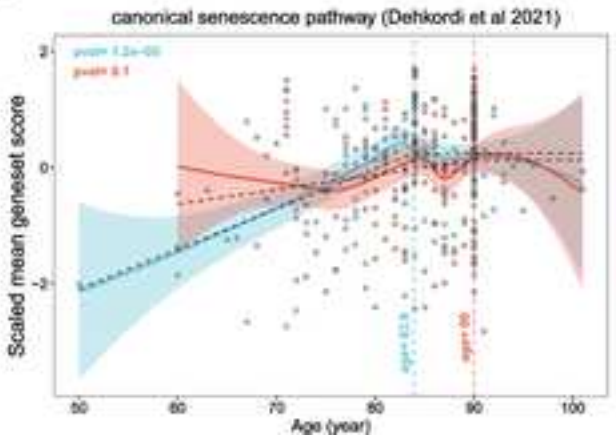

Fig S8

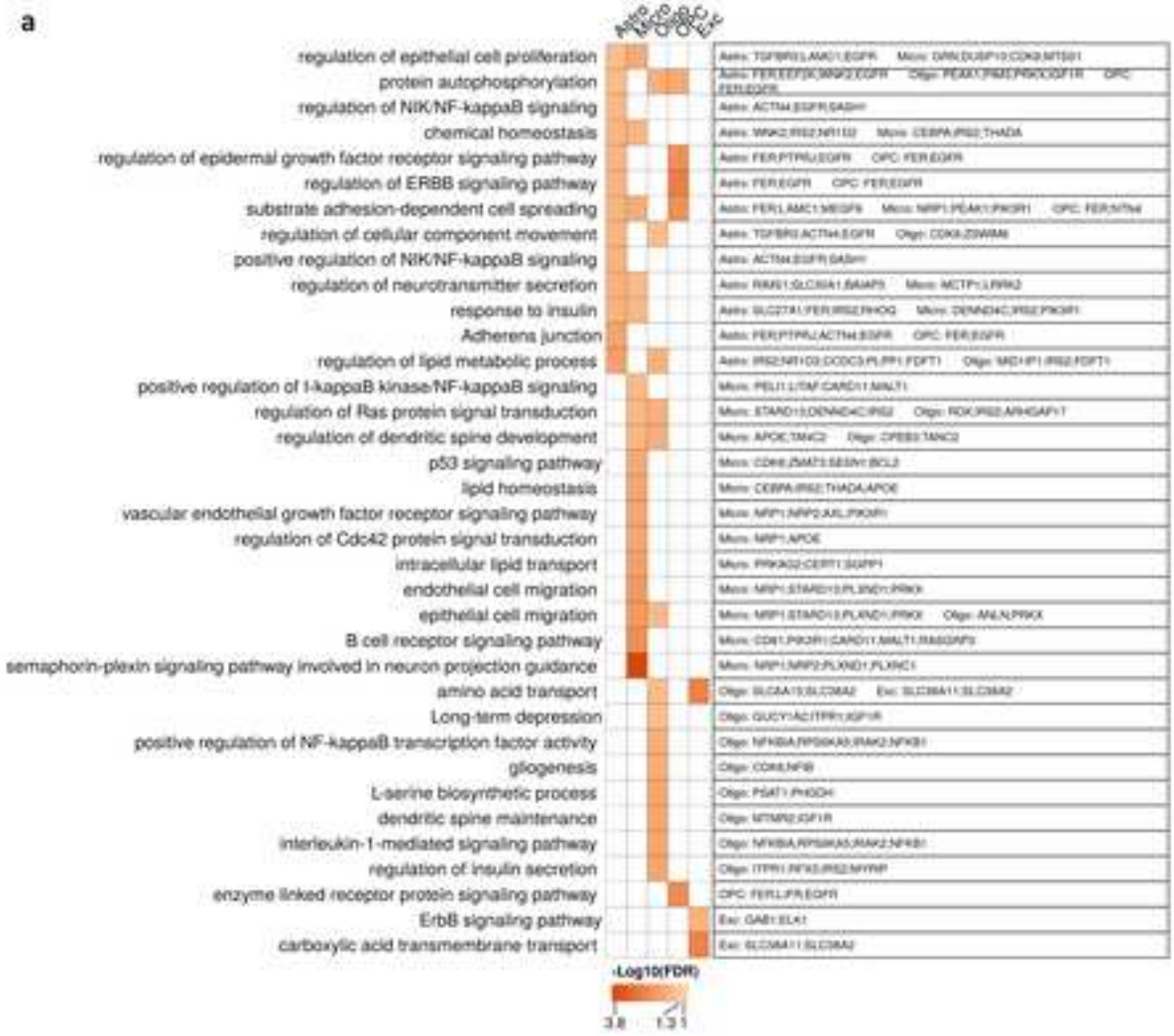
a
Astro
Micro
Oligo
OPC
Exc
regulation of epithelial cell proliferation
protein autophosphorylation
regulation of NIK/NF-kappaB signaling
chemical homeostasis
regulation of epidermal growth factor receptor signaling pathway
regulation of ERBB signaling pathway
substrate adhesion-dependent cell spreading
regulation of cellular component movement
positive regulation of NIK/NF-kappaB signaling
regulation of neurotransmitter secretion
response to insulin
Adherens junction
regulation of lipid metabolic process
positive regulation of I-kappaB kinase/NF-kappaB signaling
regulation of Ras protein signal transduction
regulation of dendritic spine development
p53 signaling pathway
lipid homeostasis
vascular endothelial growth factor receptor signaling pathway
regulation of Cdc42 protein signal transduction
intracellular lipid transport
endothelial cell migration
epithelial cell migration
B cell receptor signaling pathway
semaphorin-plexin signaling pathway involved in neuron projection guidance
amino acid transport
Long-term depression
positive regulation of NF-kappaB transcription factor activity
gliogenesis
L-serine biosynthetic process
dendritic spine maintenance
interleukin-1-mediated signaling pathway
regulation of insulin secretion
enzyme linked receptor protein signaling pathway
ErbB signaling pathway
carboxylic acid transmembrane transport
-Log10(FDR)
3.8
1.3
1

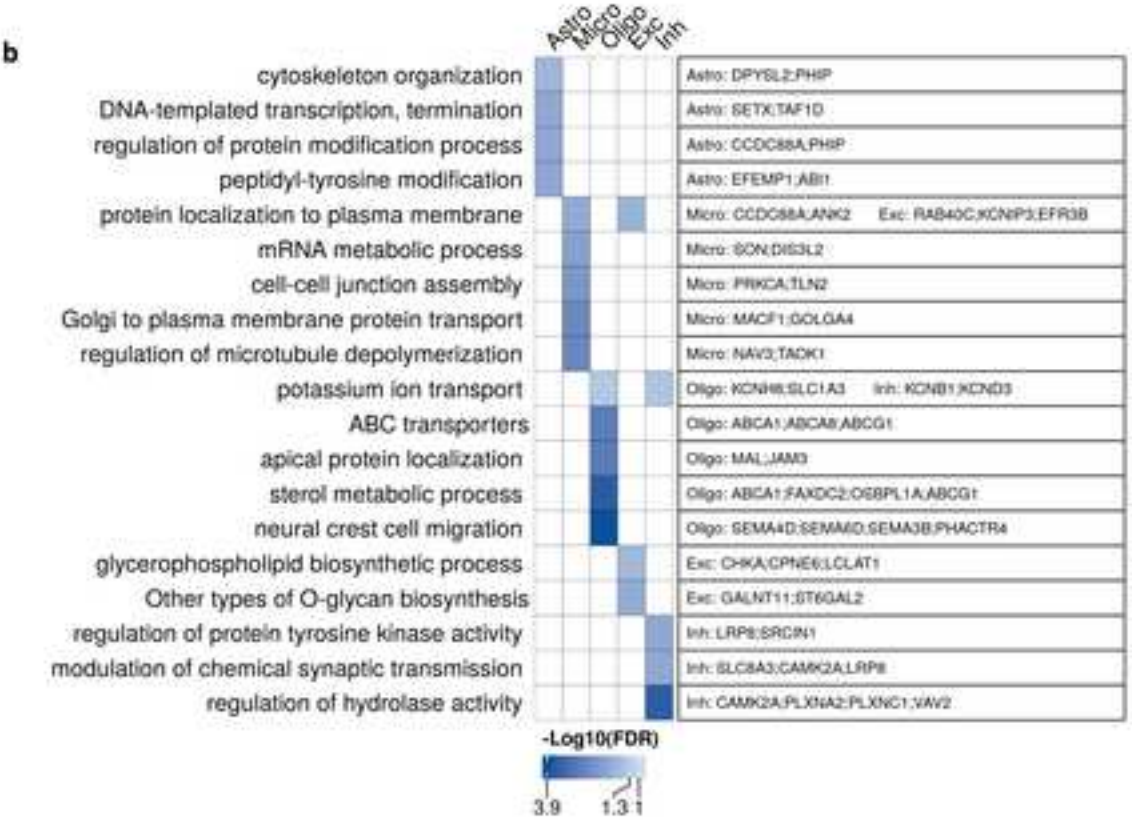
b
Astro
Micro
Oligo
Exc
Inh
cytoskeleton organization
DNA-templated transcription, termination
regulation of protein modification process
peptidyl-tyrosine modification
protein localization to plasma membrane
mRNA metabolic process
cell-cell junction assembly
Golgi to plasma membrane protein transport
regulation of microtubule depolymerization
potassium ion transport
ABC transporters
apical protein localization
sterol metabolic process
neural crest cell migration
glycerophospholipid biosynthetic process
Other types of O-glycan biosynthesis
regulation of protein tyrosine kinase activity
modulation of chemical synaptic transmission
regulation of hydrolase activity
Astro: DPYSL2;PHIP
Astro: SETX;TAF1D
Astro: CCDC88A;PHIP
Astro: EFEMP1;ABI1
Micro: CCDC88A;ANK2
Exc: RAB40C;KCNIP3;EFR3B
Micro: SON;DIS3L2
Micro: PRKCA;TLN2
Micro: MACF1;GOLGA4
Micro: NAV3;TAOK1
Oligo: KCNH8;SLC1A3
Inh: KCNB1;KCND3
Oligo: ABCA1;ABCA8;ABCG1
Oligo: MAL;JAM3
Oligo: ABCA1;FAXDC2;OSBPL1A;ABCG1
Oligo: SEMA4D;SEMA6D;SEMA3B;PHACTR4
Exc: CHKA;CPNE6;LCLAT1
Exc: GALNT11;ST6GAL2
Inh: LRP8;SRGN1
Inh: SLC8A3;CAMK2A;LRP8
Inh: CAMK2A;PLXNA2;PLXNC1;VAV2
-Log10(FDR)
3.9
1.3
1

Fig S9

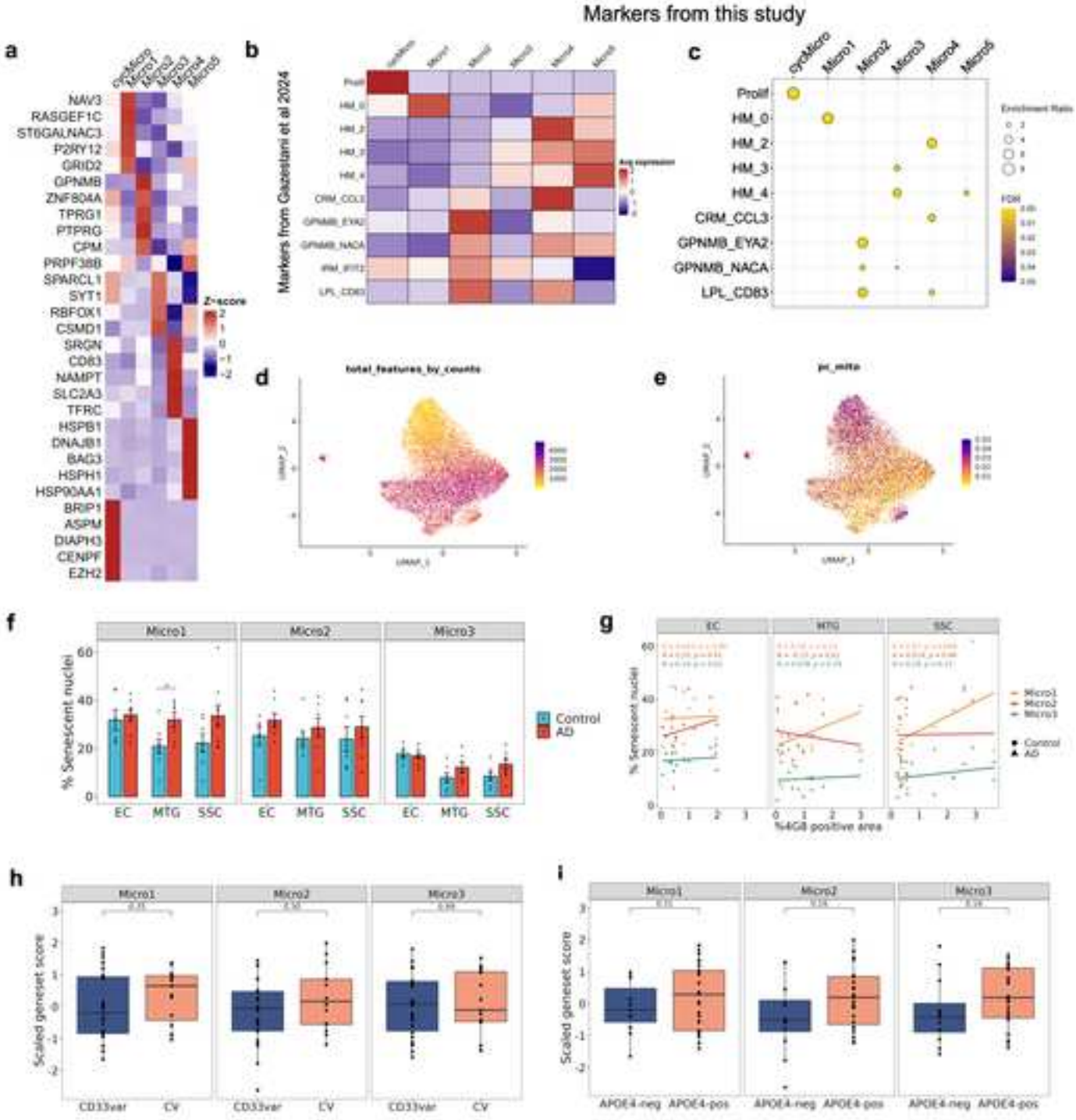
Markers from this study
a
cycMicro
Micro1
Micro2
Micro3
Micro4
Micro5
NAV3
RASGEF1C
ST6GALNAC3
P2RY12
GRID2
GPNMB
ZNF804A
TPRG1
PTPRG
CPM
PRPF38B
SPARCL1
SYT1
RBFOX1
CSMD1
SRGN
CD83
NAMPT
SLC2A3
TFRC
HSPB1
DNAJB1
BAG3
HSPH1
HSP90AA1
BRIP1
ASPM
DIAPH3
CENPF
EZH2
Z-score
b
Markers from Gazestani et al 2024
c
Prolif
HM_0
HM_2
HM_3
HM_4
CRM_CCL3
GPNMB_EYA2
GPNMB_NACA
LPL_CD83
Enrichment Ratio
FDR
d
total_features_by_counts
e
pc_mito
f
Micro1
Micro2
Micro3
% Senescent nuclei
EC
MTG
SSC
Control
AD
g
EC
MTG
SSC
% Senescent nuclei
%4G8 positive area
Micro1
Micro2
Micro3
Control
AD
h
Micro1
Micro2
Micro3
Scaled geneset score
CD33var
CV
i
Micro1
Micro2
Micro3
Scaled geneset score
APOE4-neg
APOE4-pos

Fig S10

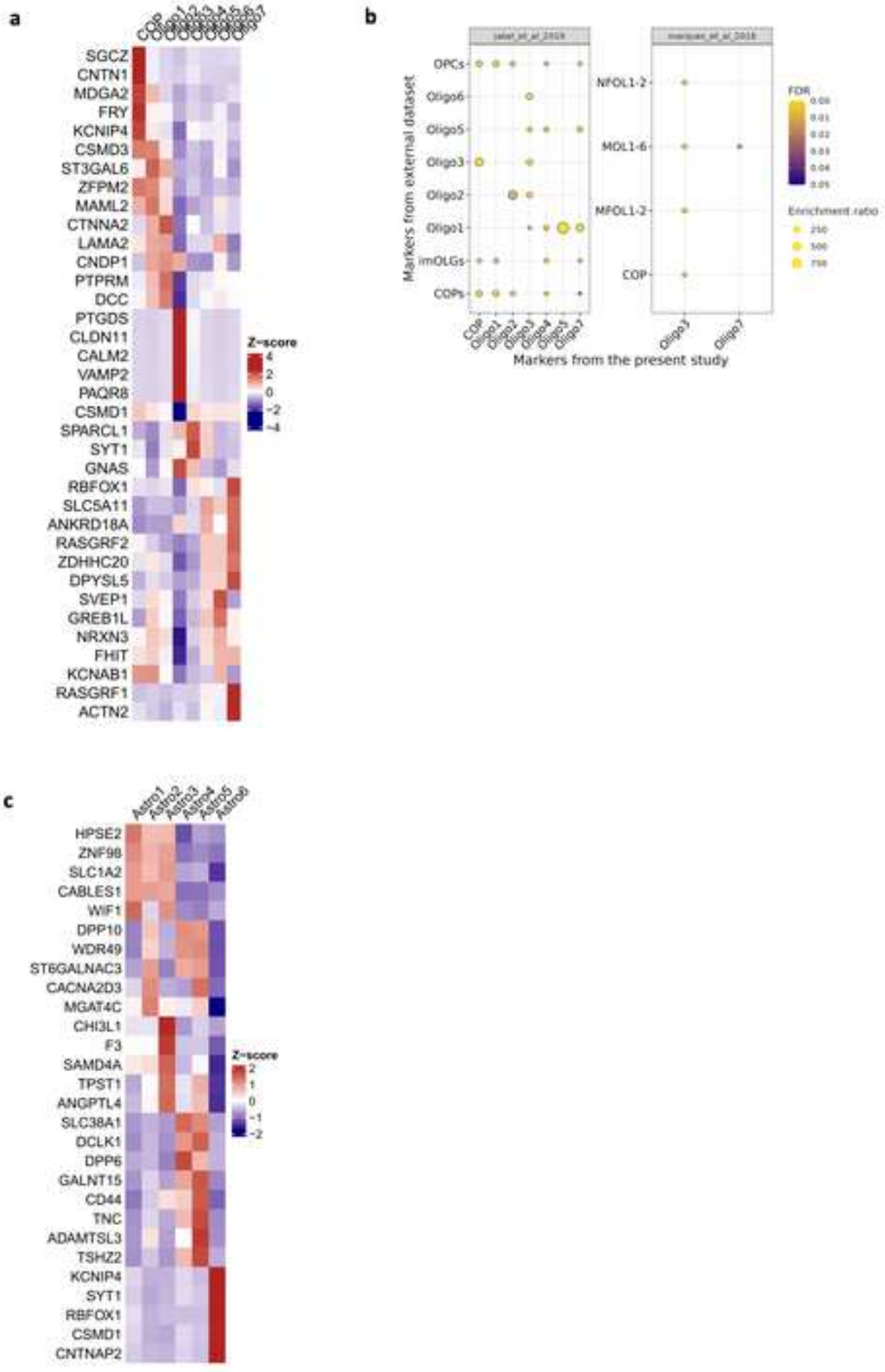
a
COP
Oligo1
Oligo2
Oligo3
Oligo4
Oligo5
Oligo6
Oligo7
SGCZ
CNTN1
MDGA2
FRY
KCNIP4
CSMD3
ST3GAL6
ZFPM2
MAML2
CTNNA2
LAMA2
CNDP1
PTPRM
DCC
PTGDS
CLDN11
CALM2
VAMP2
PAQR8
CSMD1
SPARCL1
SYT1
GNAS
RBFOX1
SLC5A11
ANKRD18A
RASGRF2
ZDHHC20
DPYSL5
SVEP1
GREB1L
NRXN3
FHIT
KCNAB1
RASGRF1
ACTN2
Z-score
4
2
0
−2
−4
b
OPCs
Oligo6
Oligo5
Oligo3
Oligo2
Oligo1
imOLGs
COPs
NFOL1-2
MOL1-6
MFOL1-2
COP
Markers from external dataset
Markers from the present study
FDR
Enrichment ratio
c
Astro1
Astro2
Astro3
Astro4
Astro5
Astro8
HPSE2
ZNF98
SLC1A2
CABLES1
WIF1
DPP10
WDR49
ST6GALNAC3
CACNA2D3
MGAT4C
CHI3L1
F3
SAMD4A
TPST1
ANGPTL4
SLC38A1
DCLK1
DPP6
GALNT15
CD44
TNC
ADAMTSL3
TSHZ2
KCNIP4
SYT1
RBFOX1
CSMD1
CNTNAP2
Z-score
2
1
0
−1
−2

Fig S11

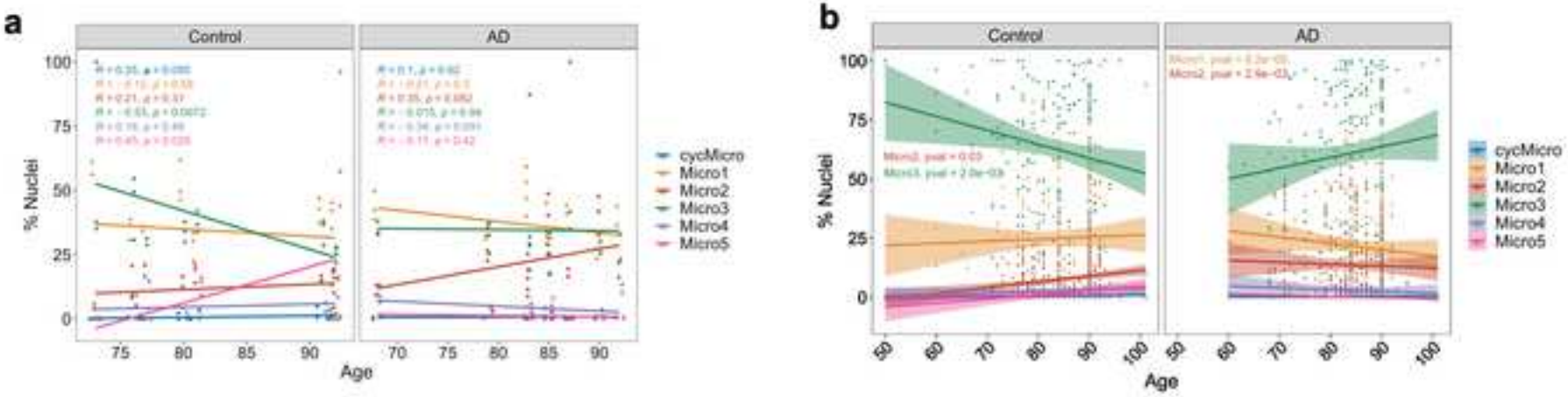
a
Control
AD
100
75
50
25
0
% Nuclei
75
80
85
90
70
75
80
85
90
Age
cycMicro
Micro1
Micro2
Micro3
Micro4
Micro5
b
Control
AD
100
75
50
25
0
% Nuclei
50
60
70
80
90
100
Age
cycMicro
Micro1
Micro2
Micro3
Micro4
Micro5

Fig S12

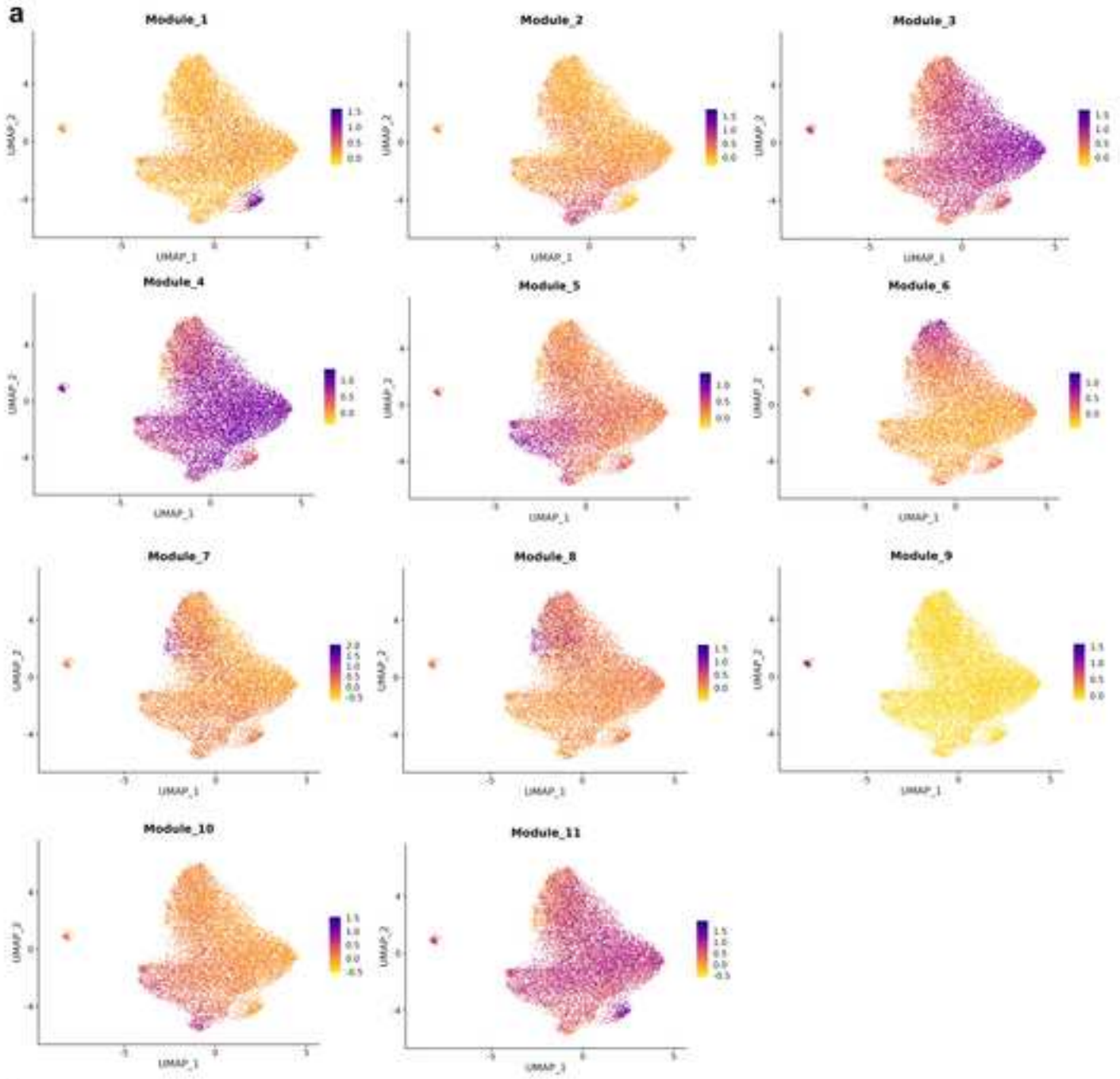
a
Module_1
Module_2
Module_3
Module_4
Module_5
Module_6
Module_7
Module_8
Module_9
Module_10
Module_11
UMAP_1
UMAP_2

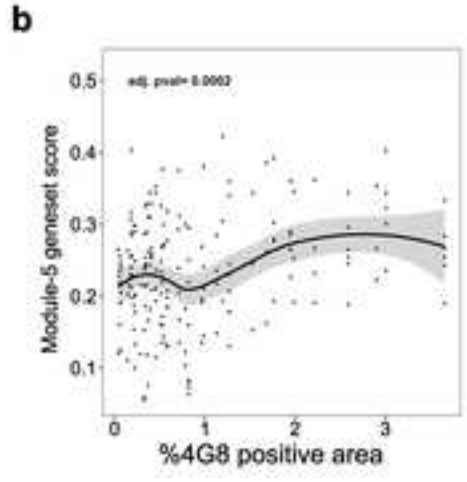
b
adj. pval= 0.0002
Module-5 geneset score
%4G8 positive area
0.1
0.2
0.3
0.4
0.5
0
1
2
3

Extended_method_fig-1